Signaling from maize organ primordia via FASCIATED EAR3 regulates stem cell proliferation and yield traits

Byoung Il Je[1], Jeremy Gruel[2,7], Young Koung Lee[1,7], Peter Bommert[1], Edgar Demesa Arevalo[1], Andrea L. Eveland[1], Qingyu Wu[1], Alexander Goldshmidt[1], Robert Meeley[3], Madelaine Bartlett[4], Mai Komatsu[5], Hajime Sakai[5], Henrik Jönsson[2,6] and David Jackson[1]

[1] Cold Spring Harbor Laboratory, Cold Spring Harbor, NY, USA.

[2] Sainsbury Laboratory, Cambridge University, Cambridge, UK.

[3] DuPont Pioneer, Agricultural Biotechnology, Johnston, IA, USA.

[4] Biology Department, University of Massachusetts, Amherst, MA, USA.

[5] DuPont Pioneer, Agricultural Biotechnology, Wilmington DE, USA.

[6] Computational Biology & Biological Physics Group, Lund University, Lund, Sweden.

[7]These authors contributed equally to this work.

Correspondence should be addressed to D. J. (jacksond@cshl.edu).

Shoot apical meristems are stem cell niches that balance proliferation with the incorporation of daughter cells into organ primordia. This balance is maintained by CLAVATA-WUSCHEL feedback signaling between the stem cells at the tip of the meristem, and the underlying organizing center. Signals that provide feedback from organ primordia to control the stem cell niche in plants have also been hypothesized, but their identity is unknown. Here we report FASCIATED EAR3 (FEA3), a leucine-rich repeat receptor that functions in stem cell control, and responds to a CLAVATA3/ESR-related (CLE) peptide expressed in organ primordia. We modeled our results to reveal a regulatory system that transmits signals from differentiating cells in organ primordia back to the stem cell niche, and that appears to function broadly in the plant kingdom. Furthermore, we demonstrate an application of this new signaling feedback, by showing that weak alleles of *fea3* enhance hybrid maize yield traits.

Stem cells occur in niches, specialized microdomains where proliferation of pluripotent cells is controlled by signals from neighboring cells[1,2]. In plants, for example, the WUSCHEL (WUS) transcription factor promotes stem cell fate, and is expressed in the organizing center cells below the stem cells. WUS activates *CLAVATA* (*CLV*) gene expression, and the CLV3 peptide signal is secreted from stem cells at the tip of the SAM, is perceived by leucine-rich repeat (LRR) receptors, such as CLV1, expressed in and above the *WUS* domain, and signals in a feedback to repress *WUS* expression[3-5].

Although such feedback systems are well described in animals and plants, it is not known if or how signals expressed in differentiating progeny cells also feedback to control the stem cell niche. In plants, such signals have been hypothesized[6-8], and consistent with this idea the inhibition of primordium growth leads to SAM enlargement[9], but the underlying molecular mechanism(s) are unknown. To search for factors controlling stem cell proliferation, we focused on maize *fasciated ear* (*fea*) mutants, some of which correspond to CLV receptors already described in dicots[10-13]. Here we provide evidence to support a new receptor-ligand signaling pathway that acts to restrict stem cell proliferation using a signal expressed in differentiating cells in organ primordia.

RESULTS

fea3 mutants have enlarged and fasciated meristems.

The *fea3* mutant arose in an irradiation mutagenesis screen, and was introgressed into the B73 background. *fea3* vegetative shoot apical meristems (SAMs) were wider (mean 150 ± 4.5μm, compared to 128 ± 5.8μm for wild type (wt) siblings, *P* value < 0.001 by 2 tailed *t* test) (**Fig. 1a, b**). Despite the larger SAM, its identity and organization was not adversely affected, as shown by *KNOTTED1* expression (**Supplementary Fig. 1a**)[14]. *fea3* mutants had prominent inflorescence defects, including thick tassels, and strongly fasciated ears with increased seed row number, resembling maize *clv* mutants (**Fig. 1c-j**)[10,13], although overall plant stature was normal (**Supplementary Fig. 1b**). In contrast to maize *clv* receptor mutants, however, spikelet and flower development was normal in *fea3* (**Supplementary Fig. 1c, d**)[10,13]. Fasciated ears and thick tassels

result from increased stem cell proliferation in inflorescence meristems. We found that *fea3* tassel inflorescence meristems were larger than wt (**Fig. 1c, d**). *fea3* ear inflorescence meristems were also enlarged, and became more severely affected during development (**Fig. 1f-i**).

FEA3, a transmembrane receptor, is expressed in the SAM.

We mapped *fea3* to a region containing ~20 genes (**Fig. 1k**), including one that encoded an LRR receptor-like protein. Based on similar phenotypes for related genes[10,13], we sequenced this locus from *fea3-0,* and found a retrotransposon fragment inserted in the second exon, introducing a premature stop codon (**Supplementary Fig. 2a**). Three additional *fea3* alleles from a targeted ethylmethane sulphonate (EMS) screen, contained amino acid substitutions relative to the progenitor (**Fig. 1l and Supplementary Fig. 2b**). Therefore *FEA3* encodes an LRR receptor-like protein, with a predicted signal peptide followed by 12 LRRs, a transmembrane domain, and a short cytoplasmic tail lacking any kinase or other predicted signaling domain (**Fig. 1l**).

FEA3 expression was enriched in meristems (**Supplementary Fig. 2c**), and *in situ* hybridization detected expression in the inner cells of the vegetative SAM central zone and cells below the central zone, as well as in leaf primordia (**Fig. 2a and Supplementary Fig. 2d**). *FEA3* was also expressed in the central region of ear spikelet meristems (**Supplementary Fig. 2f**). We next expressed FEA3-red fluorescent protein (RFP) fusions driven by the endogenous promoter. RFP was fused after the signal peptide in one construct, or at the C terminus in another (**Supplementary Fig. 3a**), and both transgenes rescued *fea3* phenotypes (**Supplementary Fig. 3b**). FEA3-RFP accumulated in the central region of the SAM (**Supplementary Fig. 3c**), consistent with the *in situ* data, but was not enriched in the plasma membrane, which might reflect endocytic trafficking, as reported for CLV1[15]. We therefore treated with D15 peptide, an endocytosis inhibitor[16], and FEA3-RFP became enriched at the cell periphery after 2hr (**Fig. 2b** and **Supplementary Fig. 3d**), and we confirmed its plasma membrane localization biochemically (**Supplementary Fig. 3e**). FEA3-RFP was detected in the inner layers of the inflorescence SAM (Fig. 2b) in a pattern similar to that observed for FEA3 mRNA in the vegetative SAM (Fig. 2a), starting from the 5-6th layer below the L1 to the 12-13th

layer of cells. Expression was also found in tassel and ear inflorescence meristems, in spikelet meristems (**Supplementary Fig. 3f-h**), in leaf primordia (inset, Fig. 2b) and in cells above the quiescent center of the root (**Supplementary Fig. 3i**).

Since FEA3 was expressed lower down in the SAM compared to known Arabidopsis CLV signaling components[12,17], we investigated its effect on WUS expression. CLV3 and CLV1 are expressed above and overlapping with the *WUS* domain, and WUS expression expands upwards in *clv* mutants[3,4]. We generated a maize *WUS* reporter using the *ZmWUS1* promoter and 3' region[18] to drive a nuclear RFP. In wt plants, p*ZmWUS1-NLS.RFP* expression was in the predicted organizing center, as expected, starting 4-5 cell layers below the L1, and extending down ~5 cell layers (**Fig. 2c**), in a domain that largely overlapped with FEA3-RFP, though FEA3-RFP expression also extended lower down, below the organizing center. Strikingly, p*ZmWUS1-NLS.RFP* expression expanded downwards in *fea3,* below the presumptive organizing center (**Fig. 2d**). Interestingly, despite this obvious downward spread of p*ZmWUS1* reporter expression, there was no expansion into the upper layers of the SAM (**Fig. 2d**), suggesting that FEA3 functions to suppress *ZmWUS1* expression specifically in the region below the organizing center.

***fea3* showed resistance to a novel CLE peptide, ZmFCP1.**

As FEA3 encoded an LRR receptor-like protein, we reasoned that it might perceive CLV3 or a CLV3 related (CLE) peptide. We therefore treated seedlings with peptides, and measured root growth inhibition[19,20]. Maize roots treated with a control, scrambled CLV3 peptide (sCLV3) grew normally, but were inhibited in the presence of CLV3[21]. However, *fea2* (maize *clv2*) mutant roots showed resistance to CLV3 peptide, suggesting that FEA2 functions in CLV3 perception. *fea3* mutants, however, did not show resistance to CLV3 (**Supplementary Fig. 4**), suggesting FEA3 might perceive a different ligand. We constructed a phylogeny of maize CLV3/ESR-related (ZmCLE) peptides[22] (**Supplementary Fig. 5**), and the closest to CLV3 were ZmCLE7 and 14, and rice FLORAL ORGAN NUMBER2 (FON2)[23]. Sister to this clade, we identified a gene orthologous to rice *FON2-LIKE CLE PROTEIN1 (FCP1)*[24], that we named *ZmFCP1*. Rice *fcp1* mis-expression lines have

meristem size phenotypes, but genetic evidence suggests that the rice CLV1 ortholog is not the FCP1 receptor[24]. The predicted peptides encoded by these genes, and additional related peptides were tested, and each of them inhibited wt root growth, similar to CLV3. Interestingly, *fea3* roots showed resistance only to ZmFCP1 peptide (**Supplementary Fig. 6**). We next asked if FEA3 showed similar specificity for ZmFCP1 peptide in the shoot, by measuring its effect on SAM size in cultured embryos[21]. Wt embryos grew normally in the presence of the scrambled CLV3 peptide control, but showed significant decrease of SAM size in presence of ZmFCP1 or related peptides, such as ZmCLE7 or ZmCLE14, whereas *fea3* again showed resistance only to ZmFCP1 (**Fig. 3a, b**). These findings suggest that FEA3 functions as a receptor in perception of the ZmFCP1 peptide. In contrast, *fea2* mutants showed resistance to a broader class of peptides, including CLV3, ZmFCP1 and ESR2c, consistent with findings for *clv2* in *Arabidopsis* (**Supplementary Fig. 6b**).

In *Arabidopsis, CLV3* is expressed in stem cells at the tip of the SAM, and it is believed that CLV3 peptide moves down towards the organizing center to restrict WUS expression[3-5], although the peptide itself has never been localized *in vivo*. In contrast to *CLV3*, we found that *ZmFCP1* was not expressed in the SAM, but in leaf primordia and in cells on the flank of the SAM that are destined to be incorporated into primordia (**Fig. 3c,** for comparison of *FEA3* and *ZmFCP1* expression see **Supplementary Fig. 7a, b**). We next obtained a *Mutator* insertion[25] in the first exon of *ZmFCP1*, and homozygous mutants had a fasciated ear phenotype (**Fig. 3d**). *Zmfcp1* vegetative SAMs were also wider than normal (mean 167 ± 10.4μm, compared to 142 ± 7.5μm for wt siblings; *P* value < 0.001), and *fea3* was epistatic to *Zmfcp1*, as the double mutants had the same SAM size as *fea3* single mutants (**Fig. 3e, f**).

In summary, our data support the idea that *ZmFCP1* controls SAM size in the same pathway as *FEA3*. We propose a model in which ZmFCP1 peptide is produced from differentiating primordium cells, and suppresses WUS expression and stem cell proliferation via the FEA3 receptor in the SAM. This model is supported by FEA3 and ZmFCP1 expression patterns, and by our observation of downward spread of WUS in *fea3* mutant meristems.

Computational modeling of *FEA3-ZmFCP1* interactions.

To understand the spatial patterning resulting from this new CLE-peptide/ receptor signaling, we integrated the *FEA3*/ *ZmFCP1* regulation of *ZmWUS1* with the canonical *CLV3/WUS* feedback loop, recently modeled in *Arabidopsis*[26-28] (**methods, Supplementary Fig. 7-12**). We assumed that certain functions and expression domains, such as for cytokinin genes, *WUS* and its activation of stem cells, are conserved in maize, though some of these have not been demonstrated yet. On a 3D geometry representing the maize SAM and two primordia (**Supplementary Fig. 7-12**), the model reproduced the wt expression domain of *ZmWUS1*, and could generate a stem cell domain expressing a hypothetical *ZmCLV3* ortholog at the central zone (**Fig. 4a**). The model predicts that a mutation in the FEA3 receptor that responds to a CLE signal from the leaf primordia, leads to downward spread of *ZmWUS1* expression, and that this would lead to an expansion of the stem cell population and up-regulation of CLV3 expression, which has previously been correlated to fasciation[3,29]. We tested this model in three ways. First, we measured expression of *ZmCLE7*, a maize ortholog of *CLV3* (**Supplementary Fig. 5**), and found an increase in expression in meristem tips of *fea3* mutants (**Supplementary Fig. 13**), consistent with our predictions. Next, we characterized *fea3; fea2* double mutants, and found highly synergistic phenotypes in ear inflorescence meristem size, or tassel spikelet density (P value < 0.001), a proxy for tassel inflorescence meristem size[21] (**Fig. 4b, c**), suggesting *FEA3* and *FEA2* act in different pathways that may converge on the same downstream target, consistent with our model (**Fig. 4a**). As a third test of the model, we overexpressed *ZmFCP1* in organ primordia using a two-component driver system[30]. We used a *pYABBY14-LhG4* line to drive primordium specific expression of a *pOp-ZmFCP1* responder line. Driver specificity was confirmed by detection of *pOp-NLS.RFP* only in primordia (**Supplementary Fig. 14a, b**), and we measured SAM size in segregating families. Plants carrying either driver or responder components alone had normal SAM size, but plants carrying both constructs showed strong inhibition of SAM growth (**Fig. 4d-g**), and ZmFCP1 over-expression was confirmed by qRT-PCR (**Supplementary Fig. 14c**). These tests of the model support the idea that ZmFCP1 signaling from differentiating primordia is sufficient

to suppress stem cell proliferation, consistent with a reduced WUS expression domain in the *fcp1* over-expression model (**Fig. 4a**).

***Arabidopsis FEA3* ortholog mutants are also fasciated.**

To ask if *FEA3* was specific to maize, we characterized its three potential orthologs, *At1g68780*, *At1g13230* and *At3g25670* in *Arabidopsis* (**Supplementary Fig. 5).** Predicted null T-DNA mutants of the first two showed no obvious phenotype, even when combined in a double mutant. We therefore made artificial microRNA (**Supplementary Fig. 15a, b**) or RNAi lines for the third ortholog, and more than 50% of the RNAi plants showed fasciated inflorescence stems (**Fig. 5b, c**). RNAi specificity for *At3g25670* (hereafter called *AtFEA3*), was confirmed by qRT-PCR (**Supplementary Fig. 15c**). As expected, the SAMs of these RNAi lines were enlarged (strong lines 294 ± 24µm, weak lines 85 ± 12µm, compared to 67 ± 7.6µm in wt; *P* value < 0.001) (**Fig. 5d, e**). However, in contrast to known *clv* mutants[31-33], but similar to maize *fea3*, flower and silique development was normal (**Supplementary Fig. 15d-f**). This might explain why this mutant has not been characterized previously, since it doesn't show the silique/ flower phenotypes typical of *clv* mutants. We also asked if *AtFEA3* RNAi plants showed altered sensitivity to CLE peptides[19]. Interestingly, as in maize, the *AtFEA3* RNAi lines did not show resistance to CLV3, but were resistant to a related CLE peptide, CLE27, in roots and in the SAM (**Fig. 5f, g**). *CLE27* is not the *ZmFCP1* ortholog (**Supplementary Fig. 5**), however it is expressed similarly, at the SAM periphery and not in the central zone (**Supplementary Fig. 15g**). Our results indicate that FEA3 function is conserved in *Arabidopsis*, and that it may perceive a CLE peptide that is produced in cells that are programmed for differentiation.

***fea3* weak alleles enhance hybrid maize yield traits.**

We previously found that weak alleles of fasciated ear mutants could improve maize yield traits, such as kernel row number[34], by increasing meristem size and number of primordia while maintaining structural integrity of the meristem. To ask if *fea3* weak alleles have similar effects, we

backcrossed EMS alleles developed in our non-complementation screen to W22 or B73 inbred lines, and generated F1 hybrids. As expected, the B73/ W22 wt hybrids had significantly enhanced yields compared to the inbreds, due to heterosis. We found that *fea3-2* and *fea3-3* weak allele hybrids further enhanced ear length, kernel row number, kernel number per ear and ear weight (**Fig. 6a-f** and **Supplementary Table 1**). The weak alleles were mildly fasciated, but did not display the stunted ear growth that is normally associated with strongly fasciated mutants. These results are particularly exciting, because in our previous studies of weak *fea2* alleles we found an increase in kernel row number but no overall increase in ear weight, due to a compensatory reduction in kernel size[34]. Therefore the newly identified *FEA3* signaling pathway could be used to develop new alleles for crop improvement.

DISCUSSION

Our results reveal a conserved signaling system that has fundamentally different expression patterns and receptor/ peptide combination compared to the well-characterized *CLV-WUS* system. We hypothesize that this system allows feedback control of SAM size using a CLE signal expressed in differentiating primordia. Our model suggests that this new CLE signal moves from the organ primordia to the SAM, where it is perceived by FEA3; however we cannot rule out the possibility of a secondary mobile signal, since the FEA3 receptor is also expressed in primordia. Indeed such a caveat also applies to CLV3, because technical limitations have precluded the localization of CLV3 peptide *in vivo*. A feedback signaling system from primordia could provide control of stem cell proliferation, and plant growth, by integrating metabolic or other signals from the developing primordia. Weak alleles of *fea3* displayed enhanced yield traits, as well as overall yield, in contrast to weak alleles of *fea2* which increase kernel number without enhancing overall yield[34], suggesting that *fea3* weak alleles might also enhance sink strength in developing ears. A recent study also highlighted the importance of feedback signaling from progeny cells to the stem cell niche in mammalian hair follicles[35], suggesting this may be a universal mechanism to control stem cell proliferation during development, with the potential to enhance crop yield traits.

URLs. Sequences and molecular markers available at MaizeGDB, http://www.maizegdb.org/; two-component driver system, http://maize.jcvi.org/cellgenomics/geneDB_list.php; FACS sorting data in the Arabidopsis eFP browser, http://bbc.botany.utoronto.ca/efp/cgi-bin/efpWeb.cgi; Python scientific package for modeling, scipy, http://www.scipy.org/.

METHODS

Methods and any associated references are available in the online version of the paper.

ACCESSION CODES. *fea3-0* sequence is available from GenBank accession number, KX009408 (http://www.ncbi.nlm.nih.gov/Genbank/).

Note: Any Supplementary Information and Source Data files are available in the Online version of the paper.

ACKNOWLEDGEMENTS

The *fea3-0* allele was kindly provided by Victor Shcherbak, Krasnodar Res. Inst. Agric., Russia. We acknowledge funding from a collaborative agreement with Dupont Pioneer, and from NSF Plant Genome Research Program grant # IOS-1238202 and MCB-1027445, and with the support of the Gatsby Charitable Foundation (GAT3395/PR4) and Swedish Research Council (VR2013-4632) to HJ, and "Next-Generation BioGreen 21 Program (SSAC, Project No. PJ01137901)" Rural Development Administration, Republic of Korea. We also thank Ulises Hernandez for assistance with cloning, Amandine Masson for assistance with peptide assays, and members of the Jackson lab for comments on the manuscript.

AUTHOR CONTRIBUTIONS

B.I.J. performed all experimental procedures, except for those listed below, prepared figures and wrote the draft of the manuscript. Y.K.L and P.B. mapped and cloned *FEA3*. J.G. performed computational modeling, supervised by H.J. E.D.A. analyzed transactivation lines, using constructs generated by Q.W. A.L.E. performed expression analyses. A.G. performed ZmWUS1 reporter line construction and characterization. R.M. provided the *ZmFCP1* mutants. M.B. performed phylogenetic analyses. M.K. and H.S. provided field genetics and mapping support and analysis. D.J. supervised the research and co-wrote the manuscript.

COMPETING FINANCIAL INTERESTS

The authors (B.I.J., Y.K.L., D.J. M.K. and H.S., on behalf of Cold Spring Harbor Laboratory and DuPont Pioneer) have obtained a patent US20150047071 A1 based in part on this work with the US Patent and Trademark Office.

References

1. Morrison, S.J. & Spradling, A.C. Stem cells and niches: mechanisms that promote stem cell maintenance throughout life. *Cell* **132**, 598-611 (2008).
2. Heidstra, R. & Sabatini, S. Plant and animal stem cells: similar yet different. *Nat Rev Mol Cell Biol* **15**, 301-12 (2014).
3. Brand, U., Fletcher, J.C., Hobe, M., Meyerowitz, E.M. & Simon, R. Dependence of stem cell fate in Arabidopsis on a feedback loop regulated by CLV3 activity. *Science* **289**, 617-9 (2000).
4. Schoof, H. *et al.* The stem cell population of Arabidopsis shoot meristems is maintained by a regulatory loop between the CLAVATA and WUSCHEL genes. *Cell* **100**, 635-644 (2000).
5. Stahl, Y. & Simon, R. Plant primary meristems: shared functions and regulatory mechanisms. *Curr Opin Plant Biol* **13**, 53-8 (2010).
6. Emery, J.F. *et al.* Radial patterning of Arabidopsis shoots by class IIIHD-ZIP and KANADI genes. *Current Biology* **13**, 1768-1774 (2003).
7. Goldshmidt, A., Alvarez, J.P., Bowman, J.L. & Eshed, Y. Signals derived from YABBY gene activities in organ primordia regulate growth and partitioning of Arabidopsis shoot apical meristems. *Plant Cell* **20**, 1217-1230 (2008).
8. Tanaka, W. *et al.* The YABBY gene TONGARI-BOUSHI1 is involved in lateral organ development and maintenance of meristem organization in the rice spikelet. *Plant Cell* **24**, 80-95 (2012).
9. Scanlon, M.J. The polar auxin transport inhibitor N-1-naphthylphthalamic acid disrupts leaf initiation, KNOX protein regulation, and formation of leaf margins in maize. *Plant Physiol* **133**, 597-605 (2003).
10. Taguchi-Shiobara, F., Yuan, Z., Hake, S. & Jackson, D. The fasciated ear2 gene encodes a leucine-rich repeat receptor-like protein that regulates shoot meristem proliferation in maize. *Genes & Development* **15**, 2755-2766 (2001).
11. Jeong, S., Trotochaud, A.E. & Clark, S.E. The Arabidopsis CLAVATA2 gene encodes a receptor-like protein required for the stability of the CLAVATA1 receptor-like kinase. *Plant Cell* **11**, 1925-34 (1999).
12. Clark, S.E., Williams, R.W. & Meyerowitz, E.M. The CLAVATA1 gene encodes a putative receptor kinase that controls shoot and floral meristem size in Arabidopsis. *Cell* **89**, 575-85 (1997).
13. Bommert, P. *et al.* thick tassel dwarf1 encodes a putative maize ortholog of the Arabidopsis CLAVATA1 leucine-rich repeat receptor-like kinase. *Development* **132**, 1235-45 (2005).
14. Jackson, D., Veit, B. & Hake, S. Expression of Maize Knotted1 Related Homeobox Genes in the Shoot Apical Meristem Predicts Patterns of Morphogenesis in the Vegetative Shoot. *Development* **120**, 405-413 (1994).

15. Nimchuk, Z.L., Tarr, P.T., Ohno, C., Qu, X.A. & Meyerowitz, E.M. Plant Stem Cell Signaling Involves Ligand-Dependent Trafficking of the CLAVATA1 Receptor Kinase. *Current Biology* **21**, 345-352 (2011).
16. Luscher, C. *et al.* Role of AMPA receptor cycling in synaptic transmission and plasticity. *Neuron* **24**, 649-658 (1999).
17. Fletcher, J.C., Brand, U., Running, M.P., Simon, R. & Meyerowitz, E.M. Signaling of cell fate decisions by CLAVATA3 in Arabidopsis shoot meristems. *Science* **283**, 1911-4 (1999).
18. Nardmann, J. & Werr, W. The shoot stem cell niche in angiosperms: Expression patterns of WUS orthologues in rice and maize imply major modifications in the course of mono- and dicot evolution. *Molecular Biology and Evolution* **23**, 2492-2504 (2006).
19. Kondo, T. *et al.* A plant peptide encoded by CLV3 identified by in situ MALDI-TOF MS analysis. *Science* **313**, 845-848 (2006).
20. Ito, Y. *et al.* Dodeca-CLE peptides as suppressors of plant stem cell differentiation. *Science* **313**, 842-5 (2006).
21. Bommert, P., Je, B.I., Goldshmidt, A. & Jackson, D. The maize Galpha gene COMPACT PLANT2 functions in CLAVATA signalling to control shoot meristem size. *Nature* **502**, 555-8 (2013).
22. OpsahlFerstad, H.G., LeDeunff, E., Dumas, C. & Rogowsky, P.M. ZmEsr, a novel endosperm-specific gene expressed in a restricted region around the maize embryo. *Plant Journal* **12**, 235-246 (1997).
23. Suzaki, T. *et al.* Conservation and diversification of meristem maintenance mechanism in Oryza sativa: Function of the FLORAL ORGAN NUMBER2 gene. *Plant Cell Physiol* **47**, 1591-602 (2006).
24. Suzaki, T., Yoshida, A. & Hirano, H.Y. Functional diversification of CLAVATA3-related CLE proteins in meristem maintenance in rice. *Plant Cell* **20**, 2049-58 (2008).
25. McCarty, D.R. & Meeley, R.B. Transposon resources for forward and reverse genetics in maize. in *Handbook of Maize: Genetics and Genomics.* (eds. Bennetzen, J.L. & Hake, S.C.) 561-584 (Springer Press, 2009).
26. Yadav, R.K. *et al.* Plant stem cell maintenance involves direct transcriptional repression of differentiation program. *Mol Syst Biol* **9**, 654 (2013).
27. Chickarmane, V.S., Gordon, S.P., Tarr, P.T., Heisler, M.G. & Meyerowitz, E.M. Cytokinin signaling as a positional cue for patterning the apical-basal axis of the growing Arabidopsis shoot meristem. *Proc. Natl. Acad. Sci. U.S.A.* **109**, 4002-7 (2012).
28. Gruel, J. *et al.* An epidermis-driven mechanism positions and scales stem cell niches in plants. *Sci. Adv.* **2**, e1500989 (2016).
29. Kinoshita, A. *et al.* RPK2 is an essential receptor-like kinase that transmits the CLV3 signal in Arabidopsis. *Development* **137**, 3911-20 (2010).
30. Wu, Q., Luo, A., Zadrozny, T., Sylvester, A. & Jackson, D. Fluorescent protein marker lines in maize: generation and applications. *Int J Dev Biol* **57**, 535-43 (2013).
31. Clark, S.E., Running, M.P. & Meyerowitz, E.M. Clavata1, a Regulator of Meristem and Flower Development in Arabidopsis. *Development* **119**, 397-418 (1993).
32. Clark, S.E., Running, M.P. & Meyerowitz, E.M. Clavata3 Is a Specific Regulator of Shoot and Floral Meristem Development Affecting the Same Processes as Clavata1. *Development* **121**, 2057-2067 (1995).
33. Kayes, J.M. & Clark, S.E. CLAVATA2, a regulator of meristem and organ development in Arabidopsis. *Development* **125**, 3843-3851 (1998).
34. Bommert, P., Nagasawa, N.S. & Jackson, D. Quantitative variation in maize kernel row number is controlled by the FASCIATED EAR2 locus. *Nat Genet* **45**, 334-7 (2013).
35. Hsu, Y.C., Li, L. & Fuchs, E. Transit-amplifying cells orchestrate stem cell activity and tissue regeneration. *Cell* **157**, 935-49 (2014).

Figure Legends

Figure 1 *fea3* mutant phenotypes and gene identification. (**a**) Cleared SAMs of wild type (WT); *fea3* shows increased diameter (arrows) (**b**). (**c**) SEM image of wild type tassel primordium (inflorescence meristem shaded yellow); *fea3* tassel shows enlarged inflorescence meristem (**d**). (**e**) Wild type tassel (left); *fea3* tassel (right) has a thicker appearance. (**f**,**g**) Side and top-down SEM views of wild type ear primordia. (**h**,**i**) *fea3* ear primordia, showing enlargement and fasciation of inflorescence meristems. (**j**) Wild type ear (left) shows regular kernel rows; *fea3* ear (right) shows fasciation and irregular rows. (**k**) Map-based cloning of *fea3*, numbers of recombinants/F2 individuals indicated. (**l**) FEA3 is a predicted receptor like protein with a signal peptide (SP) followed by 12 LRRs, and a transmembrane domain (TM). The position of the *fea3-0* insertion and the EMS alleles are shown. Scale bars a, b = 100 µm, others = 500 µm.

Figure 2 Expression of *FEA3* and *ZmWUS1*. (**a**) *in situ* hybridization of *FEA3* shows expression in lower layers (predicted organizing center, square bracket) of the vegetative SAM and below it. (**b**) In the inflorescence apex, FEA3-RFP (red) is expressed similarly. Note that the diffuse and speckled red signal in the L1 SAM layer (*) is background auto-fluorescence. FEA3-RFP is also expressed in leaf primordia (inset). An inflorescence transition stage SAM showing *pZmWUS1-NLS.RFP* expression (red) in presumptive organizing center in wild type (**c**); expression expands downwards in *fea3* (**d**). (**b**-**d**) counterstained (blue) with calcofluor white cell wall marker (**b**-**d** = confocal microscopy). All scale bars = 50 µm.

Figure 3 Interactions between FEA3 and its putative ligand, ZmFCP1. (**a**,**b**) *fea3* embryos cultured with control, scrambled peptide (sCLV3) or ZmFCP1 or ESR2c or ZmCLE7 or ZmCLE14. Wild type SAM growth was strongly inhibited by all peptides except sCLV3, and *fea3* was insensitive only to ZmFCP1. (**c**) *in situ* hybridization of *ZmFCP1*, expression was specific to primordia (arrowed). (**d**) Zmfcp1 mutant; red arrow shows position of *Mu* transposon insertion downstream of the ATG in the first exon. *Zmfcp1* mutants have a fasciated ear phenotype, seen in top-down SEM view. (**e**) Cleared SAMs of wild type, *fea3* and *Zmfcp1*; SAMs of *fea3* and *Zmfcp1* were significantly wider (arrowed), but double mutants were not significantly different from *fea3* (**f**). Scale bars d = 500 µm, others = 50µm. n = 20 for each genotype, mean values ± s.d. are plotted; ***P* value < 0.001 by two-tailed, two-sample *t* tests; NS = not significant.

Figure 4 Computational model and test of FEA3 function. (**a**) Computational model predicting effect of genetic perturbations on a hypothetical *ZmCLV3* or *ZmWUS1* expression, and feedback up-regulation of *ZmCLV3*, see text for details. The model predictions are tested as follows: *fea2* and *fea3* act synergistically in double mutants, in ear meristems (upper images, SEM) and tassels (lower images) (**b**), and quantified by tassel spikelet density (**c**). (**d**) Trans-activated overexpression of ZmFCP1 in primordia led to severe SAM size reduction (**e**-**g**). Scale bars b = 500 µm, others = 50µm. n = 20 (**c**) and 15 (**g**), mean values ± s.d. are plotted; ***P* value < 0.001 by two-tailed, two-sample *t* tests; NS = not significant.

Figure 5 *Arabidopsis FEA3* mutants are fasciated. (**a**) Wild type *Landsberg erecta* (*Ler*) plant and SEM image of SAM (shaded, **d**). (**b**,**c**) *AtFEA3* RNAi transgenic plants were fasciated, with split inflorescence stems (arrowed), and SEM image of enlarged SAMs (shaded, **e**). (**f**) Root growth was strongly inhibited by CLE peptides, except sCLV3 control, but *AtFEA3* RNAi lines showed resistance to CLE27 (root tips marked by white lines). (**g**) Wild type SAM growth was significantly inhibited by CLE27 peptide treatment, but *AtFEA3* RNAi plants were resistant to CLE27. n = 20 (**f**) and 19 (**g**), mean values ± s.d. are plotted; ***P* value < 0.001 by two-tailed, two-sample *t* tests; NS = not significant. Scale bars **d**,**g** = 50 µm, **e** = 200µm.

Figure 6 Yield traits of *fea3* weak alleles. (**a**) *fea3* weak alleles hybrids had longer and wider ears than normal hybrids, and an increase in kernel row number (**b**, **c**, kernel rows numbered in b and quantified in c). (**d**,**e**) kernel number per ear and ear weight were also significantly higher in *fea3-2* or

fea3-3 hybrids, compared to normal hybrids. n = 20, mean values ± s.d. are plotted; **P value < 0.001 by two-tailed, two-sample t tests; NS = not significant. Greek letters indicate significant differences, bars sharing the same letter are not significantly different.

ONLINE METHODS

Plant growth and map based cloning. Maize plants were grown in the field or in the greenhouse. The original *fea3* allele, *fea3-0*, in an unknown genetic background, was crossed to the B73 inbred and selfed to make the F2 population for bulked segregant mapping. 1,000 mutants from the segregating F2 population were used for map-based cloning using molecular markers available from MaizeGDB (*fea3-0* genotype data from F2 mapping population are provided in **Supplementary data set 1**). Phenotyping used the *fea3-0* allele, backcrossed 7 times to the B73 inbred line. Additional alleles were identified using targeted EMS mutagenesis. To measure meristem size, segregating siblings were genotyped and shoot apical meristems of 14-day-old plants (**Fig. 1a, b** and **Fig. 4e, f**) or 28-day-old plants (**Fig. 3e**) were dissected, cleared and measured as described previously[10]. All measurements for all experiments described in this manuscript included at least 10 samples of each genotype, and two or three independent biological replicates, and mean values +/- s.d. were presented, with significance calculated using two-tailed, two-sample *t* tests, and significant differences reported as *P* values.

Meristem imaging and *in situ* hybridization. Scanning electron microscopy was performed on fresh tissues of maize and fixed tissues of *Arabidopsis* using a Hitachi S-3500N SEM, as described[10]. *In situ* hybridization experiments were performed as described[14]. Antisense RNAs of *FEA3* and *ZmFCP1* were transcribed and used as probes. Primers are listed in **Supplementary Table 2**.

Transgene construction and imaging. The FEA3-RFP transgene was constructed by amplification of genomic fragments and fusing the RFP gene in-frame after the signal peptide, or at the C-terminal position, and transformed into maize. We used the MultiSite Gateway System (Invitrogen). All fragments were amplified using PhusionTaq polymerase (Finnzymes) and transferred to the pTF101 Gateway compatible maize transformation vector by the multisite LR recombination. Confirmed clones were transferred to *Agrobacterium* and transformed into maize, as described[36]. Primers are

listed in **Supplementary Table 2**. To determine whether the FEA3-RFP construct could complement the *fea3-0* allele, primary FEA3-RFP transformants were crossed to homozygous *fea3-0* mutant plants, and F1 plants that carried the FEA3-RFP transgene were backcrossed to homozygous *fea3-0* mutants. Transgenic plants of these families were randomly sib-crossed and resulting families subsequently analyzed for complementation. For genotyping, a 2.14 kb fragment of the *fea3-0* locus was amplified; the equivalent amplicon was 1.96 kb fragment in wild type. The 1.96 kb PCR fragment also contained the site of RFP insertion, which allowed for simultaneous PCR detection of the transgene. The presence of the transgene locus was additionally monitored by Basta-treatment of leaf tips. The *ZmWUS1* domain marker was developed by sub-cloninig 1,576bp upstream of the GRMZM2G047448 gene ATG and 1125 bp downstream of the stop codon into the MultiSite Gateway System (Invitrogen). For nuclear localized fluorescent marker, four repeats of the Vir-E2 NLS sequence[37] were cloned in frame in front of the mRFP[38] and subsequently sub-cloned into the MultiSite Gateway System. Primers are listed in **Supplementary Table 2**.

For confocal microscopy, tissues were dissected, counterstained with calcoflour white according to manufacture instructions (Sigma-Aldrich 18909) for 2 min and imaged with a Zeiss LSM 710 microscope, using 561nm laser excitation and 570–620nm emission for RFP and 405nm laser excitation and 450-500 emission for calcoflour-white. Some tissues were treated with 2 μM D15 peptide [16] (peptide is listed in **Supplementary Table 3**) for 2hr prior to imaging.

Double mutant analysis. Double mutants were constructed by crossing mutants introgressed into B73, followed by selfing or backcrossing to the F1. All plants were subsequently genotyped (Primers are listed in **Supplementary Table 2**). Plants were scored for spikelet density by counting the number of spikelets in a 2 cm region of the tassel central spike, after 2 cm had been removed from the tip. All genotype data for the double mutant analysis are provided in **Supplementary data set 1**.

Protein extraction and detection. Aqueous two-phase partitioning was performed as described[21], using extracts from 1-2 cm maize ear primordia. To inhibit endocytosis, ear primordia were sliced into

~ 2mm pieces and were treated with 1mM D15 peptide for 2hr, or a mock treatment with 1mM randomized 15-mer peptide (peptide is listed in **Supplementary Table 3**) as a control. Samples from the upper and lower phases, enriched for plasma membrane or endoplasmic reticulum, respectively, were subjected to SDS–PAGE and western blotting. Blots were probed with antisera for RFP (Chromotek 5F8), or BiP lumenal binding protein (Agrisera AS09-481), or plasma membrane H+ ATPase (Agrisera AS07-260), and detected using a secondary HRP coupled antibody (GE), according to the manufacturer's instructions. This experiment was performed with 2 independent biological replicates.

Phylogenetic analysis. Amino acid sequences of CLE proteins from *A. thaliana*, maize, and rice were aligned using MUSCLE and the resulting alignment transferred to DNA[39]. Only a very short region of the CLE proteins could be aligned with confidence, thus the final alignment included only the functional ligand (**Supplementary Table 3**) plus two amino acids on either side. The DNA alignment (**Supplementary data set 2**) was partitioned into 1st, 2nd and 3rd coding positions, and the best-fitting model of sequence evolution and partitioning scheme was identified using PartitionFinder[40]. The alignment was analyzed both in its entirety, and as two smaller alignments, corresponding to two frequently recovered clades. All alignments were analyzed using MrBayes v3.2.4, with model parameters allowed to vary between data partitions[41]. Two independent runs were initiated in each MrBayes analysis, and both were allowed to run for 10,000,000 generations. The independent runs converged (standard deviation of split frequencies <0.01) in all analyses.

Peptide assays. Maize embryos segregating for *fea3* and wild type were dissected at 10 days after pollination, when the SAM was exposed, and cultured on gel media[21] containing scrambled peptide (30 μM; Genscript) or ZmFCP1 peptide or ESR2c peptide or ZmCLE7 peptide or ZmCLE14 peptide (peptides are listed in **Supplementary Table 3**). After 10 days, embryos were harvested for genotyping, and fixed in FAA (10%, formalin, 5% acetic acid, 45% ethanol) and cleared in methyl salicylate, and SAMs measured by microscopy. Experiments used at least 10 embryos per genotype,

and were replicated in triplicate. For measurement of root growth, mature seeds (**Supplementary Fig. 4**) or maize embryos dissected at four weeks after pollination segregating for the wild type and *fea3* mutant (**Supplementary Fig. 6a**) or segregating for *fea3;fea2* double mutants (**Supplementary Fig. 6b**) were germinated on gel media overnight. Synchronized germinating embryos were selected and transferred to gel media in glass test tubes containing scrambled peptide (sCLV3; 5 μM or 10 μM, Genscript) or ESR2c peptide or ZmFCP1 peptide or AtCLV3 peptide or ZmCLE7 peptide or CLE20 peptide or CLE40 peptide or ZmCLE21 peptide or ZmCLE23 peptide (peptides are listed in **Supplementary Table 3**). After 7 days, root length was measured, and experiments were replicated in triplicate.

For measurement of *Arabidopsis* roots, sterilized seeds were cultured on half MS media containing scrambled peptide (sCLV3; 1μM) or AtCLV3 peptide or AtCLE25 peptide or AtCLE26 peptide or AtCLE27 peptide or AtCLE45 peptide (peptides are listed in **Supplementary Table 3**). After 10 days, root length was measured, and the experiment was replicated in triplicate. For the measurement of *Arabidopsis* SAMs, sterilized seeds were cultured on half MS liquid media, containing CLV3 (1μM) or sCLV3 or CLE27 and the media was renewed every third day. After two weeks, samples were harvested, fixed, cleared, and SAMs measured by microscopy. Peptide assays were completed with biological replicates performed by different investigators, and meristems were measured in a random order, before grouping based on genotype.

Two-components transactivation assay. The *pYABBY14-LhG4* driver line was constructed using a *ZmYABBY14* promoter (2697bp)[42] to drive LhG4 expression, and and the *pOp-ZmFCP1* reporter line used the complete *ZmFCP1* coding region (925bp). Fragments were cloned using the MultiSite Gateway System (Invitrogen), as shown in **Supplementary Fig. 8a**[43]. Driver and reporter line heterozygotes were crossed to each other and the two-component segregating families were analyzed. Primers are listed in **Supplementary Table 2**. For real time qPCR, dissected shoot apices (~ 2 x 2 x 3mm) including SAM and young leaves were used.

Computational methods. The model includes the *CLV3/WUS* feedback loop and is a development from recent work for *A. thaliana*[26,28,44]. It is fully described in the **Supplementary Note**.

In this system, *WUS* expression is activated by cytokinin, produced in the external cell layer[27], upon binding the AHK receptors[27,45]. The CLV3 peptide expressed in the stem cell niche represses *WUS* expression upon binding its receptor[46]; its own expression is activated by the diffusing transcription factor WUS[44].

The expression pattern of *ZmWUS1* expression in *fea3* (**Fig. 2d**) inside the meristematic tissue, and away from the epidermis, offers insights into its regulation. Interestingly, this expression pattern mirrors the expression pattern of *AHK4* in *A. thaliana*[27], suggesting that a similar cytokinin receptor could be present in maize, underlying *ZmWUS1* activation. In the following we will consider the hypothetical expression pattern of *ZmAHK4* to be the inner tissue of the SAM. When activated by cytokinin the receptor induces the expression of *ZmWUS1* in the model.

As previously shown, the positional information from the diffusion gradient of WUS alone is not sufficient to localise the *CLV3* expression domain at the tip of the shoot. In the present work, *CLV3* is co-activated by a signal originating from the epidermis allowing the gene expression domains of WUS and CLV3 to mimic their wild type (wt) expression patterns as well as those observed in a large set of mutants[26,44,47].

The model was ported to maize and adapted to include the experimental findings described in the main text. The model aims at understanding the combined CLE-signalling and the fasciation phenotype observed in the *fea3* mutant. The domain of activity of the wt *CLV3* promoter is used as a marker for the stem cell domain (central zone), and a large increase of its activity will be considered as leading to a fasciated phenotype[48].

The tissue template used for the modelling is a three-dimensional representation of the maize SAM (**Supplementary Fig. 7**). The expression domains of genes of interest are defined from experimental data: *ZmWUS1* (Fig. 2c and[18]), *ZmCLE7* (hereafter referred to as *ZmCLV3;* phylogeny in

Supplementary Fig. 5), *ZmAHK4*[49], *FEA3* (Fig. 2b), *ZmFCP1* (Fig. 3c), and also *ZmWUS1* expression in fea3 (Fig. 2d).

A schematic description of the model is shown in **Supplementary Fig. 8**. *ZmWUS1* expression is driven by cytokinin binding the ZmAHK4 receptors. FEA3 receptors upon binding ZmFCP1, and FEA2 receptors upon binding either ZmCLV3 or ZmFCP1 (as supported by peptide assays in **Fig 3a** and **Supplementary Fig. 6b**), repress *ZmWUS1* expression. *FEA2* is constitutively expressed in the model[10]. ZmWUS1 and a hypothetical epidermis-originating signal activate *ZmCLV3* expression. Gene expression is modelled using Hill functions and cell-to-cell transport of molecules is passive. The complete model is described by a set of seven differential equations for each cell of the tissue template (**Supplementary Note**).

The parameter values are inferred *via* an optimisation strategy adapted from[28] and making use of the CMA-ES algorithm[50]. Multiple optimisations resulted in 203 parameter sets successfully describing the wt expression of *ZmWUS1* and *ZmCLV3*. The model was further tested for loss of function of *ZmCLV3*, *FEA2*, *FEA3*, *FEA3; FEA2*, *FCP1* and over-expression of *FCP1*. The variation of expression of both *ZmWUS1* and *ZmCLV3* in all conditions is presented in **Supplementary Fig. 9, 10.**

fea2, *fea3* and *fea3; fea2* all lead to a substantial increase of both *ZmWUS1* and *ZmCLV3*, the model thus predicts a fasciated phenotype for the three mutants, which proves to be consistent with the experimental data presented in **Fig. 4**. Moreover, as shown, the severity of the phenotypes increases from *fea2* to *fea3* to *fea3; fea2*. Both the *fea3* and *fea3; fea2* mutants result in a large downward expansion of the *ZmWUS1* domain, similar to the *pZmWUS1-NLS.RFP* expression domain observed in *fea3* (**Fig. 2**).

fcp1 causes a large expansion of *ZmWUS1* and *ZmCLV3* and a predicted fasciated phenotype. The *ZmWUS1* domain exhibits a downward expansion typical of the *fea3* mutants.

Finally, over-expressing the *fcp1* peptide in its own expression domain (using a primordium specific YABBY promoter) causes a decrease of *ZmWUS1* expression, leading to a reduction of *ZmCLV3*

expression. The phenotype suggests a smaller stem cell pool and thus a reduction of the meristem size or meristem arrest.

The model described above is largely inspired by data obtained in *A. thaliana.* In particular, the *LOG* genes, whose expression patterns are unknown in maize, are expressed in the epidermis; in rice the expression resembles the stem cell domain[51]. In order to assess the importance of this choice we modified the model such that the production of active cytokinin would not be limited to the epidermis, but to the tip of the meristem, as suggested from the data obtained in rice.

This second "rice-like" model was optimised in the same fashion as the previous model, resulting in 295 parameter sets. Strikingly, the model behaves extremely similarly to the "Arabidopsis-like" model (**Supplementary Fig. 11, 12**), suggesting that the pattern of expression of the *LOGs* in maize could be similar to either organisms without affecting the conclusions of the present study.

***AtFEA3 RNAi* and artificial microRNA construction.** For RNAi of *At3g25670*, the full length cDNA, or the 3' untranslated region (289bp) was cloned into the pHellsgate8 (SnapGene). The precursors for artificial miRNAs against At3g25670 (TGCTCTATACATCAATGGAAA and TCGCCGATAAGAATACCTAAA) were cloned into the miR159a backbone following synthesis (Genscript) and then were mobilized into pDONR P4r-P3r. The artificial miRNAs were driven by p35S or an *AGAMOUS* promoter, pAGm[52]. We used the MultiSite Gateway System (Invitrogen). All fragments were transferred to a modified pART27 Gateway compatible arabidopsis transformation vector by the multisite LR recombination. Primers are listed in **Supplementary Table 2**. To measure meristem size, shoot apical meristems of 14-day-old plants were dissected, cleared and measured as described previously[10], n = 16 (wild type, weak lines) and 8 (strong lines).

Quantification of transcript abundance. Q-RTPCR analysis was performed on a CFX96 Real-time system (Bio-RAD), as described[53]. Total mRNAs were extracted using an RNA extraction kit (Qiagen). The target cycle threshold values were normalized using *ZmUbiquitin* or *AtActin2*. Data are presented as the mean of three biological replicates and three technical replicates. Primers are listed in

the **Supplementary Table 2**. RNA-seq reads from inflorescence meristem tips were obtained from wild type and *fea3* mutant ear primordia as previously described[54]. Two biological replicates (pools of ~30 inflorescence meristem tips) were compared between wild type and *fea3* mutants. Reads were mapped to the maize reference genome (AGPv3) using TopHat2[55] and counts were normalized by the total number of reads mapped before plotting[56].

Yield trials. *fea3* EMS alleles developed in the non-complementation screen were backcrossed to W22 or B73 2 - 4 times, and F1 homozygous mutants hybrids generated by crossing. Heterozygous *fea3-2* or *fea3-3* mutants hybrids were used as the control "normal" hybrids. Field tests were performed at Uplands Farm (Cold Spring Harbor, New York) in the summer of 2015. For analysis of yield parameters, 20-30 open-pollinated ears with full seed set were analyzed.

36. Mohanty, A. *et al.* Advancing Cell Biology and Functional Genomics in Maize Using Fluorescent Protein-Tagged Lines. *Plant Physiology* **149**, 601-605 (2009).
37. Crawford, K.M. & Zambryski, P.C. Subcellular localization determines the availability of non-targeted proteins to plasmodesmatal transport. *Curr Biol* **10**, 1032-40 (2000).
38. Osterrieder, A. *et al.* Fluorescence lifetime imaging of interactions between Golgi tethering factors and small GTPases in plants. *Traffic* **10**, 1034-46 (2009).
39. Edgar, R.C. MUSCLE: multiple sequence alignment with high accuracy and high throughput. *Nucleic Acids Res* **32**, 1792-7 (2004).
40. Lanfear, R., Calcott, B., Ho, S.Y. & Guindon, S. Partitionfinder: combined selection of partitioning schemes and substitution models for phylogenetic analyses. *Mol Biol Evol* **29**, 1695-701 (2012).
41. Ronquist, F. *et al.* MrBayes 3.2: efficient Bayesian phylogenetic inference and model choice across a large model space. *Syst Biol* **61**, 539-42 (2012).
42. Juarez, M.T., Twigg, R.W. & Timmermans, M.C. Specification of adaxial cell fate during maize leaf development. *Development* **131**, 4533-44 (2004).
43. Krishnakumar, V. *et al.* A maize database resource that captures tissue-specific and subcellular-localized gene expression, via fluorescent tags and confocal imaging (Maize Cell Genomics Database). *Plant Cell Physiol.* **56**, e12(1–7) (2015).
44. Yadav, R.K. *et al.* WUSCHEL protein movement mediates stem cell homeostasis in the Arabidopsis shoot apex. *Genes Dev* **25**, 2025-30 (2011).
45. Gordon, S.P., Chickarmane, V.S., Ohno, C. & Meyerowitz, E.M. Multiple feedback loops through cytokinin signaling control stem cell number within the Arabidopsis shoot meristem. *Proc. Natl. Acad. Sci. U.S.A.* **106**, 16529-34 (2009).
46. Ogawa, M., Shinohara, H., Sakagami, Y. & Matsubayashi, Y. Arabidopsis CLV3 peptide directly binds CLV1 ectodomain. *Science* **319**, 294 (2008).
47. Jönsson, H., Shapiro, B.E., Meyerowitz, E.M. & Mjolsness, E. Signalling in multicellular models of plant development. in *On growth, form and computers*, (eds. Sanjeev Kumar and Peter J. Bentley) 156-161 (Elsevier Academic Press, 2003).
48. Iliev, I. & Kitin, P. Origin, morphology, and anatomy of fasciation in plants cultured in vivo and in vitro. *Plant Growth Regulation* **63**, 115-129 (2011).
49. Yonekura-Sakakibara, K., Kojima, M., Yamaya, T. & Sakakibara, H. Molecular characterization of cytokinin-responsive histidine kinases in maize. Differential ligand preferences and response to cis-zeatin. *Plant Physiol* **134**, 1654-61 (2004).

50. Hansen, N. The CMA Evolution Strategy: A Comparing Review. in *Towards a new evolutionary computation. Advances in estimation of distribution algorithms.* (eds. Lozano, J.A., Larrañga, P., Inza, I. & Bengoetxea, E.) 75-102 (Springer Press, 2006).
51. Kurakawa, T. *et al.* Direct control of shoot meristem activity by a cytokinin-activating enzyme. *Nature* **445**, 652-5 (2007).
52. Hong, R.L., Hamaguchi, L., Busch, M.A. & Weigel, D. Regulatory elements of the floral homeotic gene AGAMOUS identified by phylogenetic footprinting and shadowing. *Plant Cell* **15**, 1296-309 (2003).
53. Whipple, C.J. *et al.* grassy tillers1 promotes apical dominance in maize and responds to shade signals in the grasses. *Proc. Natl. Acad. Sci. U.S.A.* **108**, E506-12 (2011).
54. Eveland, A.L. *et al.* Regulatory modules controlling maize inflorescence architecture. *Genome Res* **24**, 431-43 (2014).
55. Kim, D. *et al.* TopHat2: accurate alignment of transcriptomes in the presence of insertions, deletions and gene fusions. *Genome Biol* **14**, R36 (2013).
56. Trapnell, C. *et al.* Differential gene and transcript expression analysis of RNA-seq experiments with TopHat and Cufflinks. *Nat Protoc* **7**, 562-78 (2012).

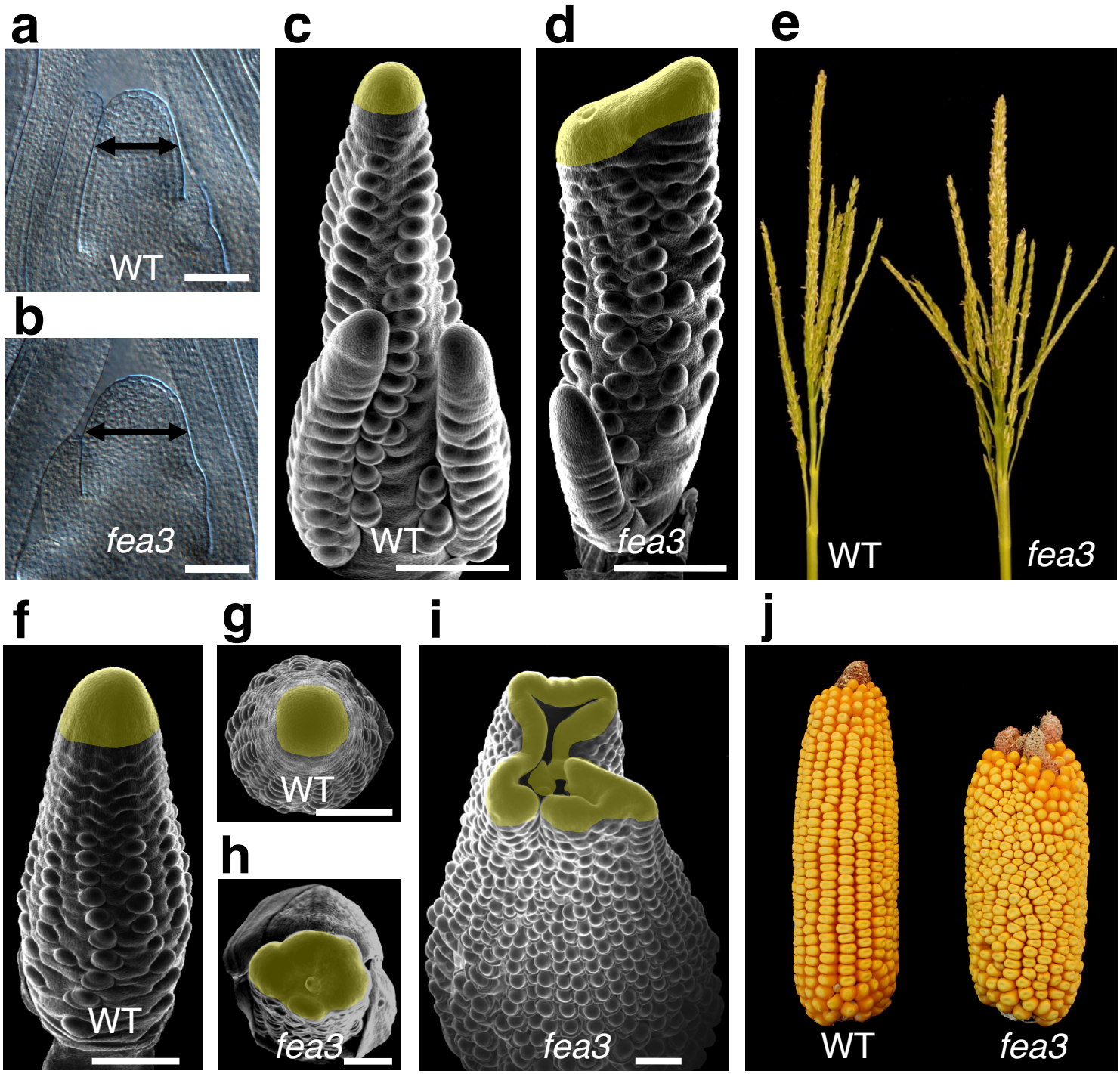
a
WT
b
fea3
c
WT
d
fea3
e
WT
fea3
f
WT
g
WT
h
fea3
i
fea3
j
WT
fea3
k Maize Chr. 3
28.9Mb
29.2Mb
29.6Mb
GRMZM2G
075320 (1/947)
FEA3
(GRMZM2G166524)
GRMZM2G
112598 (1/947)
l
S
P
12 LRRs
T
M
506aa
fea3-0
Partial retro-transposon
fea3-1
D336N
fea3-2
C417Y
fea3-3
C435Y

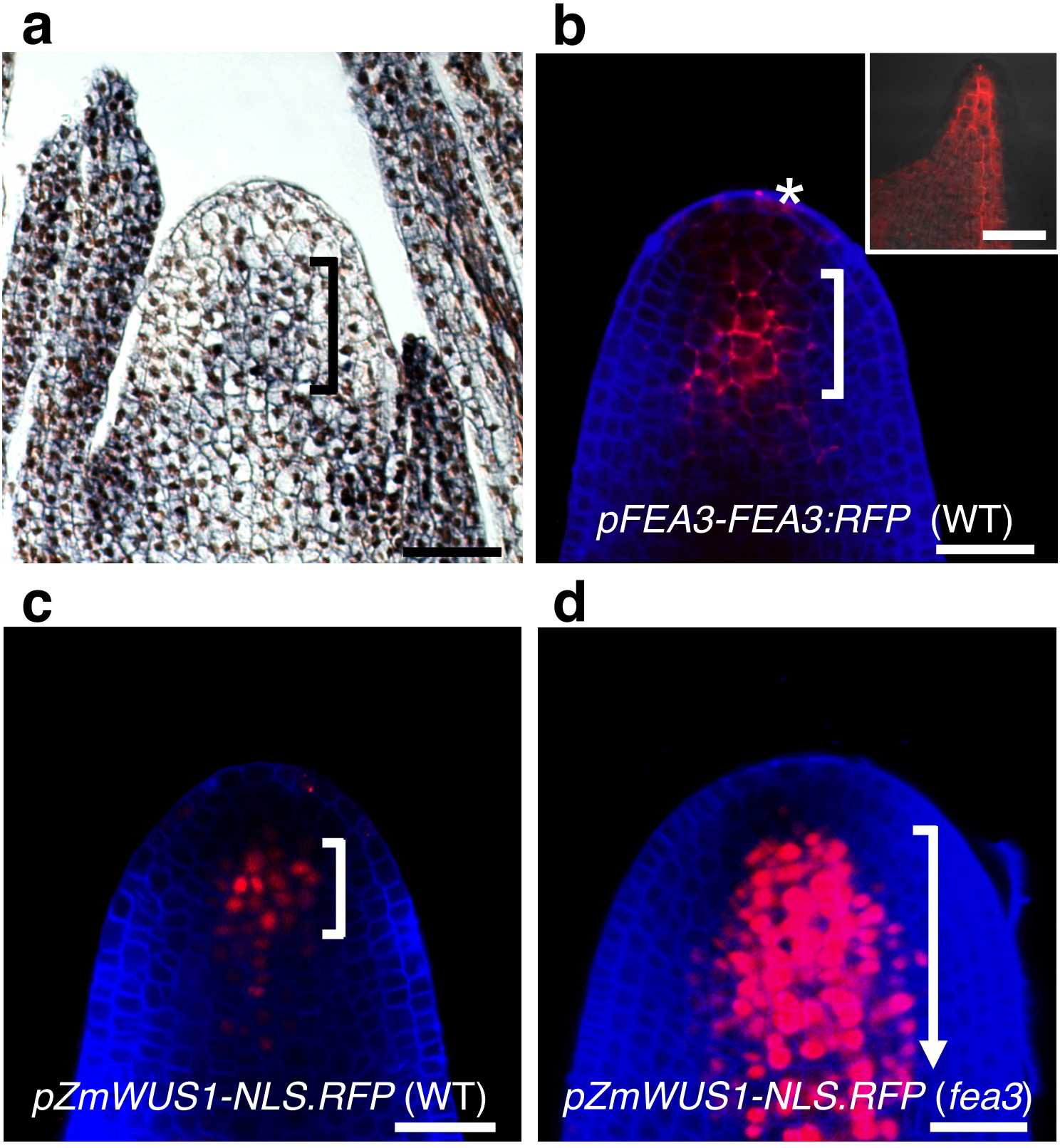
a
b
*
pFEA3-FEA3:RFP (WT)
c
pZmWUS1-NLS.RFP (WT)
d
pZmWUS1-NLS.RFP (fea3)

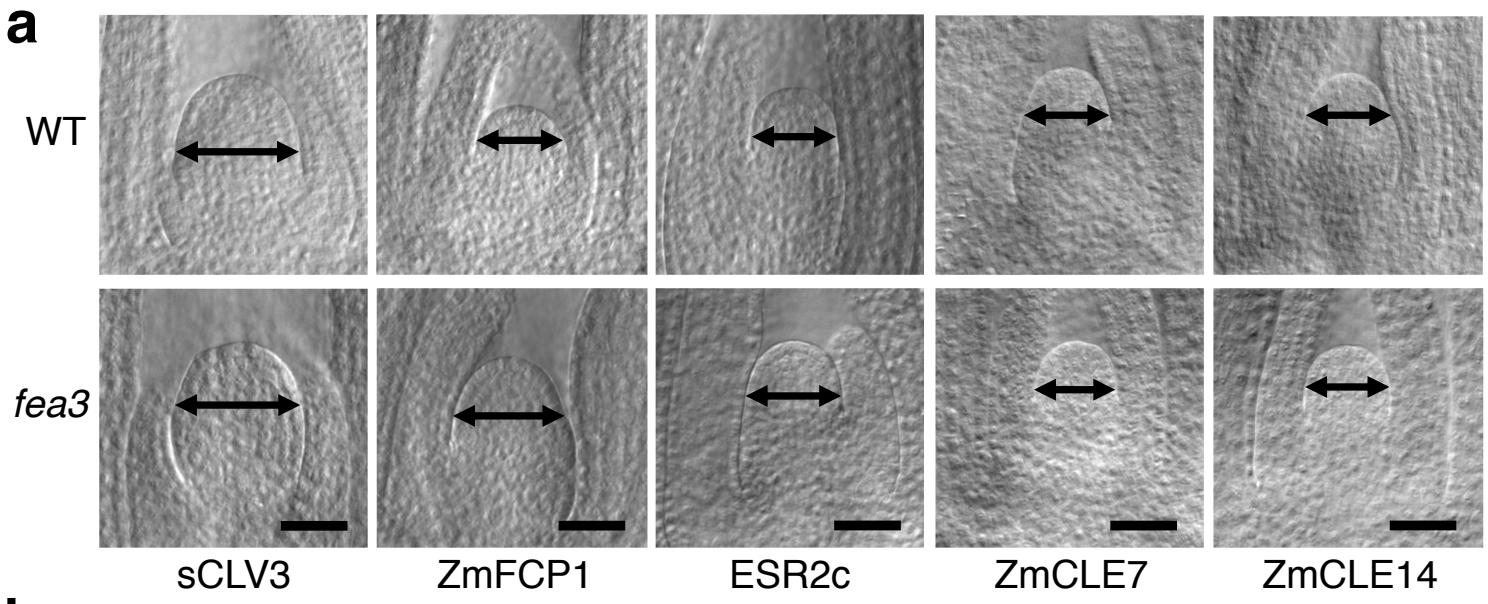
a
WT
fea3
sCLV3
ZmFCP1
ESR2c
ZmCLE7
ZmCLE14

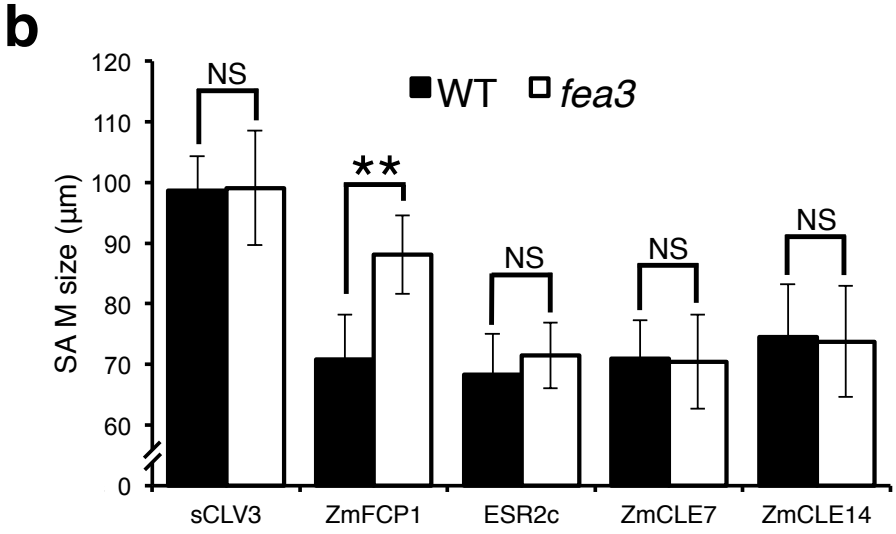
b
SA M size (µm)
120
110
100
90
80
70
60
0
NS
WT
fea3
**
NS
NS
NS
sCLV3
ZmFCP1
ESR2c
ZmCLE7
ZmCLE14

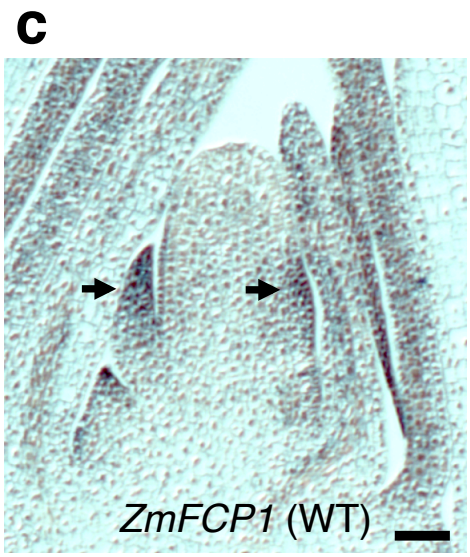
c
ZmFCP1 (WT)

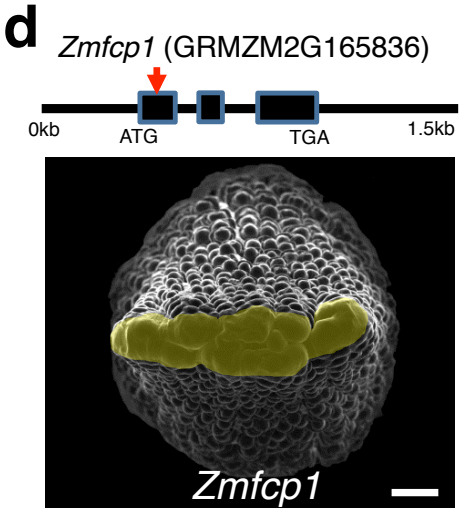
d
Zmfcp1 (GRMZM2G165836)
0kb
ATG
TGA
1.5kb
Zmfcp1

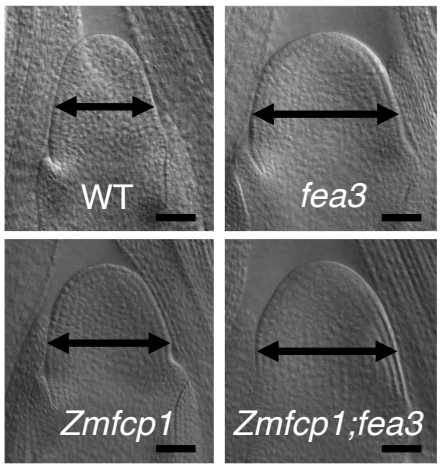
e
WT
fea3
Zmfcp1
Zmfcp1;fea3

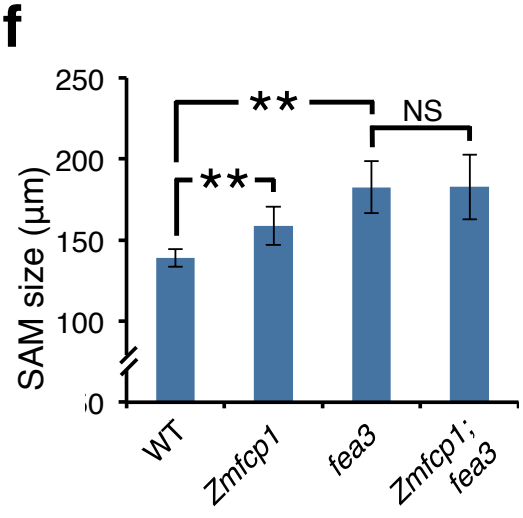
f
SAM size (µm)
250
200
150
100
50
**
**
NS
WT
Zmfcp1
fea3
Zmfcp1;
fea3

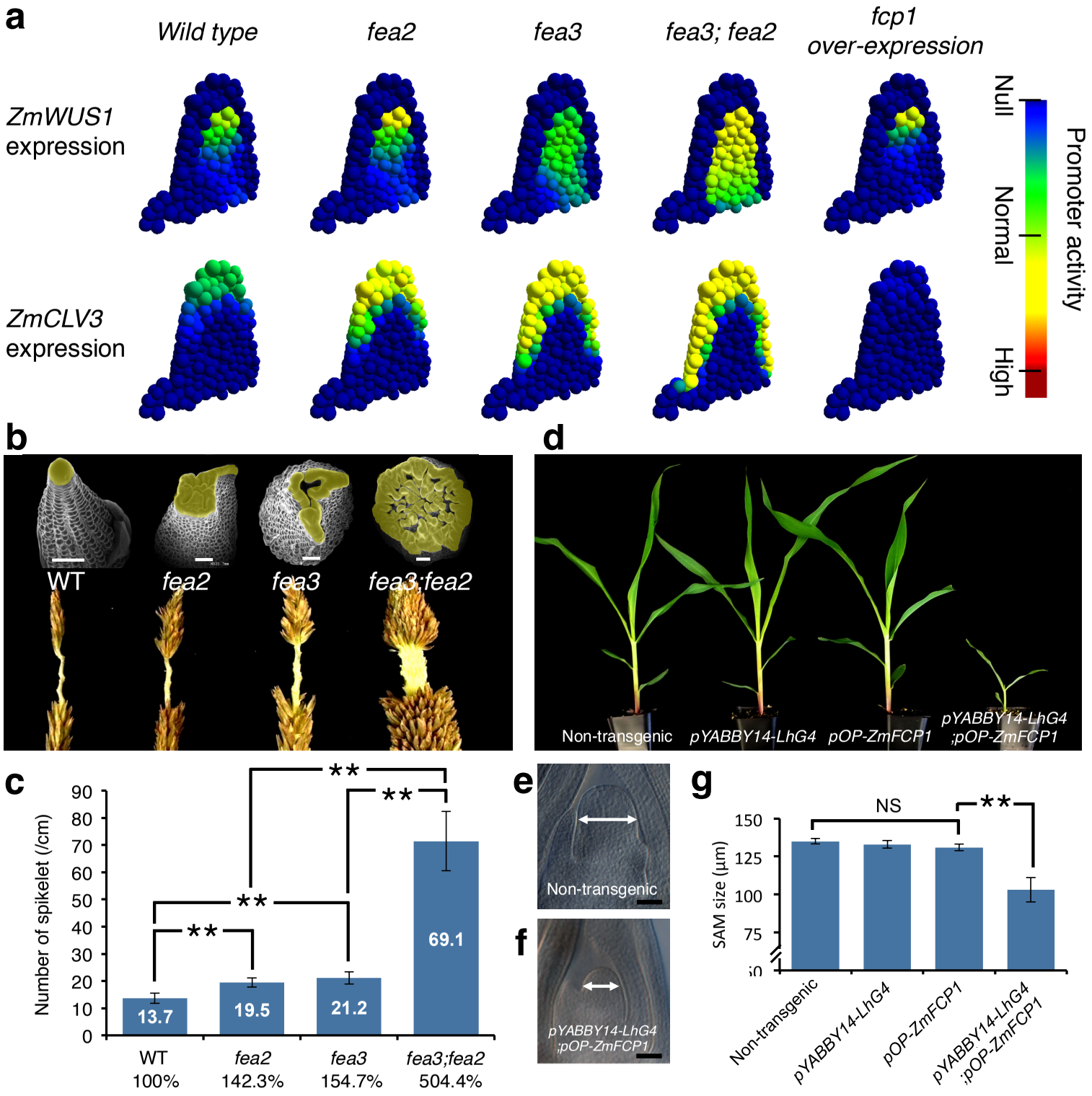
a
Wild type
fea2
fea3
fea3; fea2
fcp1 over-expression
ZmWUS1 expression
ZmCLV3 expression
Null
Normal
High
Promoter activity
b
WT
fea2
fea3
fea3;fea2
d
Non-transgenic
pYABBY14-LhG4
pOP-ZmFCP1
pYABBY14-LhG4 ;pOP-ZmFCP1
c
Number of spikelet (/cm)
13.7
19.5
21.2
69.1
**
WT 100%
fea2 142.3%
fea3 154.7%
fea3;fea2 504.4%
e
Non-transgenic
f
pYABBY14-LhG4 ;pOP-ZmFCP1
g
SAM size (μm)
NS
**
Non-transgenic
pYABBY14-LhG4
pOP-ZmFCP1
pYABBY14-LhG4 ;pOP-ZmFCP1

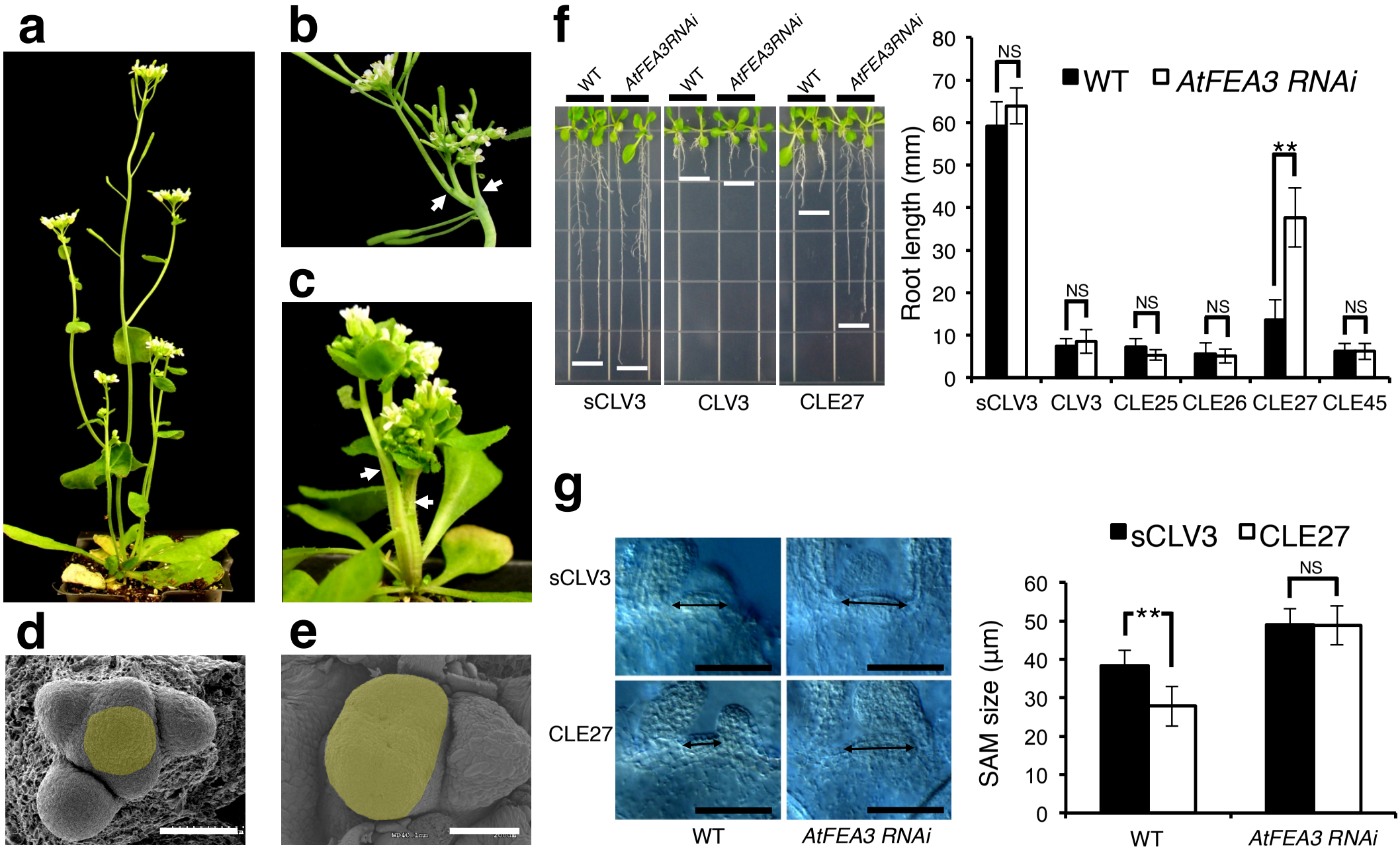
a
b
c
d
e
f
WT
AtFEA3RNAi
sCLV3
CLV3
CLE27
Root length (mm)
NS
**
CLE25
CLE26
CLE45
g
sCLV3
CLE27
WT
AtFEA3 RNAi
SAM size (μm)

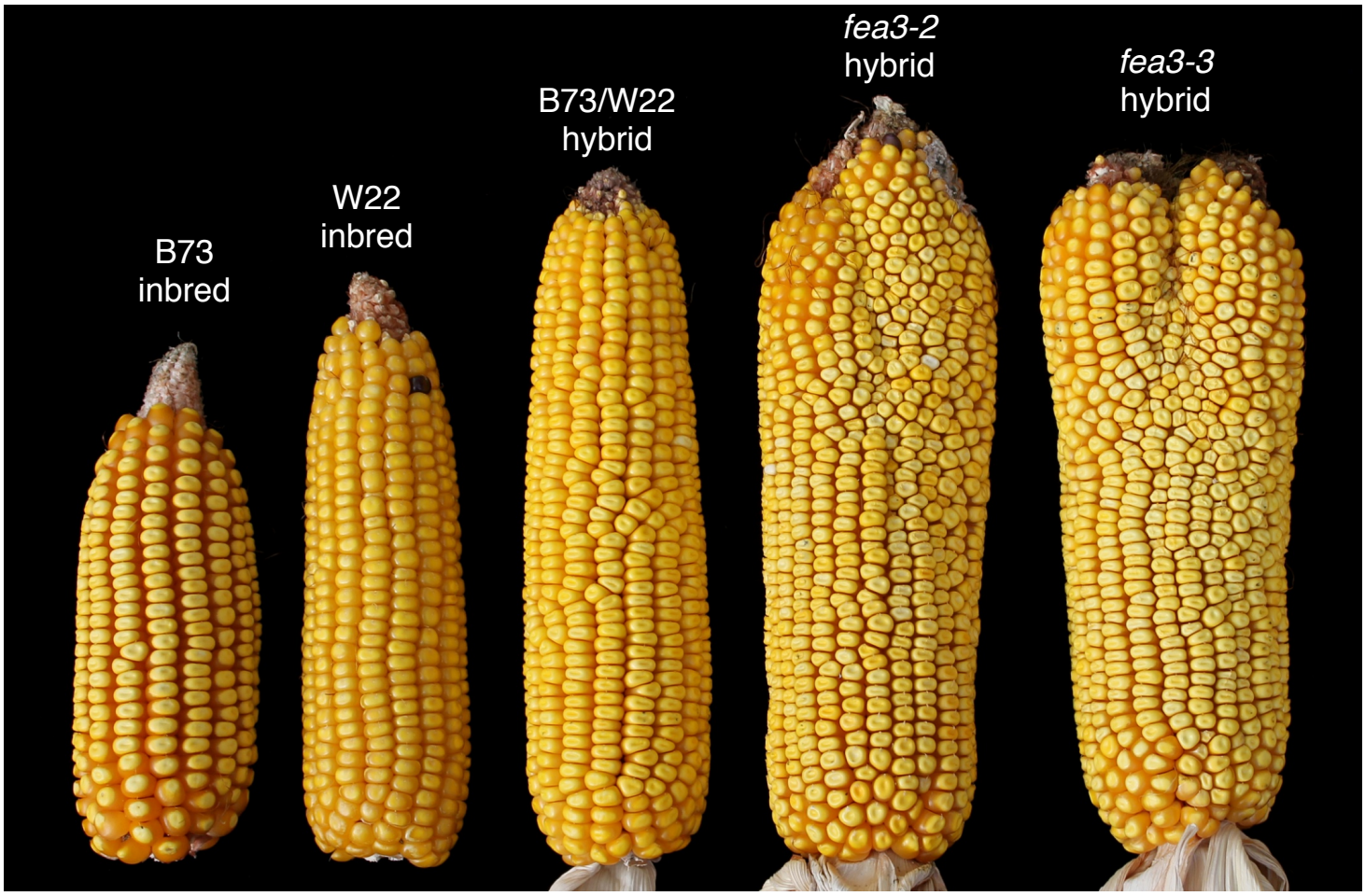
a
B73
inbred
W22
inbred
B73/W22
hybrid
fea3-2
hybrid
fea3-3
hybrid

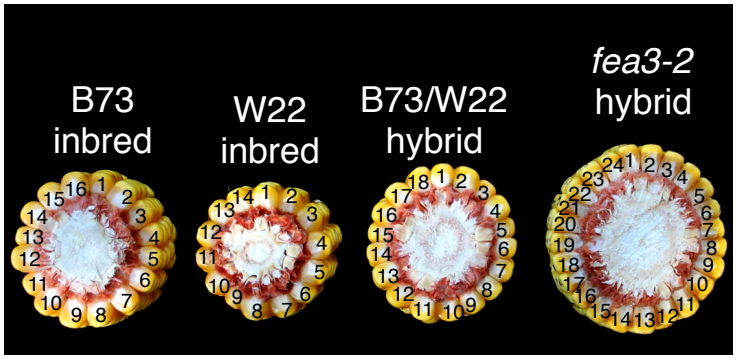
b
B73
inbred
W22
inbred
B73/W22
hybrid
fea3-2
hybrid

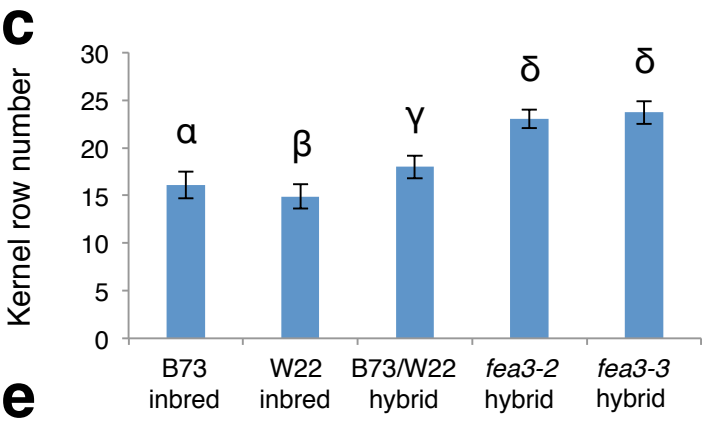
c
Kernel row number
30
25
20
15
10
5
0
α
β
γ
δ
δ
B73 inbred
W22 inbred
B73/W22 hybrid
fea3-2 hybrid
fea3-3 hybrid

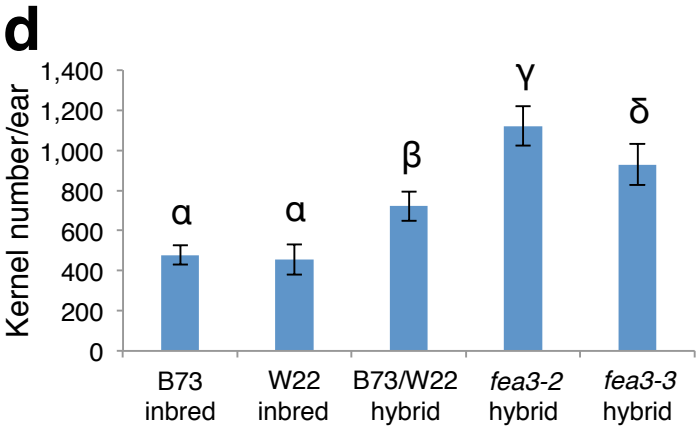
d
Kernel number/ear
1,400
1,200
1,000
800
600
400
200
0
α
α
β
γ
δ
B73 inbred
W22 inbred
B73/W22 hybrid
fea3-2 hybrid
fea3-3 hybrid

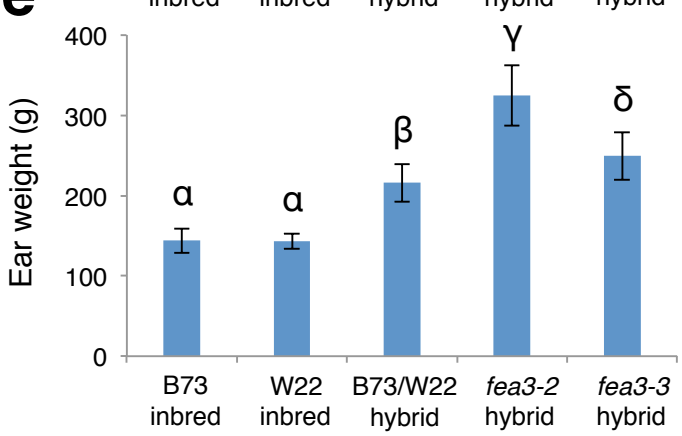
e
Ear weight (g)
400
300
200
100
0
α
α
β
γ
δ
B73 inbred
W22 inbred
B73/W22 hybrid
fea3-2 hybrid
fea3-3 hybrid

Supplementary Table 1 Summary table of yield traits.

	Ear length (cm)	Ear thickness (cm)	Kernel row number	Kernel number/row	kernel number/ear	Ear weight (g)
B73	15.03 ± 0.8 (α)	4.73 ± 0.2 (α)	16.1 ± 1.4 (α)	29.7 ± 2.3 (α)	478.6 ± 49 (α)	143.8 ± 15.1 (α)
W22	16.97 ± 0.9 (β)	4.4 ± 0.2 (β)	14.9 ± 1.3 (β)	30.4 ± 3.1 (α)	454.5 ± 76 (α)	142.1 ± 9.3 (α)
B73/W22	19.19 ± 0.9 (γ)	4.75 ± 0.3 (α)	18 ± 1.2 (γ)	42.4 ± 3.2 (β)	721.7 ± 70 (β)	215.8 ± 23.4 (β)
fea3-2 hybrid	20.29 ± 0.8 (δ)	5.73 ± 0.2 (γ)	23.03 ± 1 (δ)	45.9 ± 2.6 (γ)	1,125.0 ± 99.4 (γ)	324.6 ± 37.9 (γ)
fea3-3 hybrid	18.54 ± 0.8 (ε)	5.71 ± 0.1 (γ)	23.6 ± 1.2 (δ)	41.1 ± 3.6 (β)	929.0 ± 103 (δ)	249.2 ± 29.5 (δ)

P value < 0.001, errors represent s.d.; *n* = 20-30, values sharing the same letter in rows are not significantly different.

Supplementary Note Computational model.

The model includes the *CLV3/WUS* feedback loop and is a development from recent work for *A. thaliana*[26,28,44]. In this system *WUS* expression is activated by cytokinin, produced in the external cell layer[27], upon binding the AHK receptors[27,45]. The CLV3 peptide expressed in the stem cell niche represses *WUS* expression upon binding its receptor[46]; its own expression is activated by the diffusing transcription factor WUS[44].

The expression pattern of *ZmWUS1* expression in *fea3* (**Fig. 2d**) inside the meristematic tissue, and away from the epidermis, offers insights into its regulation. Interestingly this expression pattern mirrors the expression pattern of *AHK4* in *A. thaliana*[27], suggesting that a similar cytokinin receptor could be present in maize, underlying *ZmWUS1* activation. In the following we will consider the hypothetical expression pattern of *ZmAHK4* to be the inner tissue of the SAM. When activated by cytokinin the receptor induces the expression of *ZmWUS1* in the model.

As previously shown, the positional information from the diffusion gradient of WUS alone is not sufficient to localise the *CLV3* expression domain at the tip of the shoot. In the present work, *CLV3* is co-activated by a signal originating from the epidermis allowing the gene expression domains of WUS and CLV3 to mimic their wild type expression patterns as well as those observed in a large set of mutants[26,44,47].

The model was ported to maize and adapted to include the experimental findings described in the main text. The model aims at understanding the combined CLE-signalling and the fasciation phenotype observed in the *fea3* mutant. The domain of activity of the wild type *CLV3* promoter is used as a marker for the stem cell domain (central zone), and a large increase of its activity will be considered as leading to a fasciated phenotype[48].

Meristem tissue template

The SAM is represented by a set of spherical cells. Overlapping spheres are considered as cells in contact and can exchange diffusing molecules. The complete tissue counts 806 cells representing the shape of a maize meristem including two primordia (**Supplementary Fig. 7**). The expression domains

of genes of interest are defined from experimental data: wild type expression for *ZmWUS1* (Fig. 2c and [18]), *ZmCLE7* (hereafter referred to as *ZmCLV3;* phylogeny in **Supplementary Fig. 5**), *ZmAHK4*[49], *FEA3* (Fig. 2b), *ZmFCP1* (Fig. 3c), and also ZmWUS1 expression in *fea3* (Fig. 2d). The domains of *ZmAHK4* and *ZmCLV3* are adapted from *A. thaliana* expression domains in the SAM. Two types of boundaries are defined on the system: (i) the bottom boundary, *B*, abstracting the interface with the tissue below the meristem and where diffusing molecules are removed from simulations based on their diffusion rate, and (ii) the cells of the epidermis (*L1*) (**Supplementary Fig. 7**).

Gene expression

RNA production is modelled using Hill functions; RNAs undergo a degradation g. For a set of N_A activators $\{A_a\}$ and N_I inhibitors $\{I_b\}$, the concentration of a RNA, X, varies as:

$$\frac{dX}{dt} = V \prod_{A_a}^{N_A} \frac{A_a^n}{A_a^n + k_a^n} \prod_{I_b}^{N_I} \frac{k_b^n}{I_b^n + k_b^n} - gX$$

with V the maximal rate of RNA production. The Hill constants, k, set the required concentration of activators or inhibitors to switch a gene between its active and inactive states. The Hill coefficients, n, control the slope of the transition between states. The equilibrium of X is found for:

$$X = \frac{V \prod_{A_a}^{N_A} \frac{A_a^n}{A_a^n + k_a^n} \prod_{I_b}^{N_I} \frac{k_b^n}{I_b^n + k_b^n}}{g}$$

Diffusing molecules

Diffusing molecules are produced within a gene expression domain (*ZmWUS1*, *ZmCLV3*, *ZmFCP1*) or in the L1. This domain is referred to as P, a vector of cell RNA concentrations for gene expression or a cell vector of 1 or 0 indicating that a cell belongs to the L1 or not. The domain is associated to a production rate p. Similar to the L1, B is a vector of 1 and 0. In those cells a diffusing molecule

undergoes a degradation equal to its diffusion rate *D*. This term approximates a continued flux into the non-modelled larger tissue below the meristem. A diffusing molecule is also degraded with a rate *g*.

For a cell vector of concentrations of a diffusing molecule *X*, we have:

$$\frac{dX}{dt} = pP - gX + D\Delta X - DBX$$

where Δ is the Laplace operator; transport in the model is assumed to be passive. For a cell i with n_i neighbours $\{j\}$, the diffusion of X follows:

$$\frac{dX_i}{dt} = D\sum_{j}^{n_i}(X_j - X_i)$$

The equilibrium state of the considered molecule is found by solving the equation:

$$pP - gX + D\Delta X - DBX = 0$$

In the present study, this is achieved using the linalg.solve function of the python scientific package scipy.

Model

The complete model describes the interactions between the components of the system represented in **Supplementary Fig. 8**. ZmWUS1 expression is driven by cytokinin binding the ZmAHK4 receptors. FEA3 receptors upon binding ZmFCP1, and FEA2 receptors upon binding either ZmCLV3 or ZmFCP1 (as supported by peptide assays in **Fig 3a** and **Supplementary Fig. 6b**), repress ZmWUS1 expression. FEA2 is constitutively expressed in the model[10]. *ZmCLV3* expression is activated by ZmWUS1 and a hypothetical L1 originating signal. A schematic description of the model is shown in **Supplementary Fig. 8**.

A set of seven differential equations for each cell controls the behaviour of the genes *ZmWUS1* (*W*) and *ZmCLV3* (*C*), WUS protein (*w*), the ZmCLV3 (*c*) and ZmFCP1 (*f*) peptides, cytokinin (γ) and the L1 originating *ZmCLV3* activator (*l*), variables in brackets indicate molecular concentrations:

$$\frac{d[W]}{dt} = V_W \times \frac{([\gamma][A])^{nw}}{([\gamma][A])^{nw} + k_A^{nw}} \times \frac{k_{F_3}^{nw}}{([F_3][f])^{nw} + k_{F_3}^{nw}} \times \frac{k_{F_2}^{nw}}{([c]+[f])^{nw} + k_{F_2}^{nw}} - g_W[W]$$

$$\frac{d[w]}{dt} = p_w[W] - g_w[w] + D_w\Delta[w] - D_wB[w]$$

$$\frac{d[C]}{dt} = V_C \times \frac{[l]^{nc}}{[l]^{nc} + k_l^{nc}} \times \frac{[w]^{nc}}{[w]^{nc} + k_w^{nc}} - g_C[C]$$

$$\frac{d[c]}{dt} = p_c[C] - g_c[c] + D_c\Delta[c] - D_cB[c]$$

$$\frac{d[f]}{dt} = p_f[F] - g_f[f] + D_f\Delta[f] - D_fB[f]$$

$$\frac{d[l]}{dt} = p_lL1 - g_l[l] + D_l\Delta[l] - D_lB[l]$$

$$\frac{d[\gamma]}{dt} = p_\gamma L1 - g_\gamma[\gamma] + D_\gamma\Delta[\gamma] - D_\gamma B[\gamma]$$

A is ZmAHK4, F_3 is FEA3, F_2 is FEA2, and *F* is the *ZmFCP1*, all statically defined (**Supplementary Fig. 7**). The complete system comprises 5642 equations.

Parameter values

Since parameter values are unknown they are inferred via an optimization strategy, adapted from[28]. In order to maintain the computations linear, we propose a workaround the *CLV3-WUS* feedback loop by optimizing the system in several steps, where subparts of the network are optimized and then merged. All optimisations are carried out using the CMA-ES algorithm[50]. The strategy can be summarized as: (i) optimize the *ZmWUS1* domain using the static *ZmCLV3* domain (*Ct*) as defined in the template (**Supplementary Fig. 7**), (ii) optimize the *ZmCLV3* domain keeping the optimized *ZmWUS1* domain fixed, (iii) optimize the ZmCLV3 gradient such that the optimized *ZmCLV3* domain produces a gradient as similar as possible to the one resulting from the first step. This is followed by a confirmation step (iv), where the equilibrium of the complete optimized network is computed.

In the following, *diff(P)* will refer to computing the equilibrium concentration of a diffusing molecule across the tissue, given a production domain *P*. Similarly, *eq([*$A_1 \ldots A_{Na}$*],[*$I_1 \ldots I_{Nb}$*])* will refer to

computing the equilibrium of a gene expression regulated by *Na* activators and *Nb* inhibitors (equations above). Finally, the function *mes(X,Y,[φ,ω])* measures the difference between two vectors X and Y following: $\sum_i (X_i - Y_i)^2$, and is the main part of the cost functions used in the different steps of the optimisation strategy. If cell *i* of either vector meets the condition *φ*, the value of $(X_i\text{-}Y_i)^2$ is weighted by parameter *ω* in the final sum. The condition is used to balance the relative value of cells expressing a gene against cells not expressing it when a small proportion of the total amount of cells express the gene.

(i) *ZmWUS1* expression domain. The optimisation minimises the difference between *ZmWUS1* as defined in the template (W_t) and *ZmWUS1* (W) at equilibrium, a second component of the cost function ensures that the *ZmWUS1* domain (W_{F2}) is enlarged in *fea2* compared to wild type, and a third component that *ZmWUS1* (W_{F3}) resembles the target *ZmWUS1* domain in *fea3* (W_{tF3}). The cost function, E_W, is defined by:

$$E_W = mes(W, W_t, [W_t = 1, 5]) + mes(W_{F3}, W_{tF3}) + (0\ if \frac{\sum W_{F2}}{\sum W} < 0.75\ else\ \frac{\sum W_{F2}}{\sum W} \times 40)$$

where the summations are over all cells. Computation of *ZmWUS1* equilibrium follows:

$$f = diff(F)$$
$$c_h = diff(C_t)$$
$$W = eq([\gamma A], [(c_h + f), (F_3 \times f)])$$

ZmWUS1 equilibrium in *fea2*:

$$W_{F2} = eq([\gamma A], [(F_3 \times f)])$$

ZmWUS1 equilibrium in *fea3*:

$$W_{F3} = eq([\gamma A], [(c_h + f)])$$

The parameters k_A, k_{F3}, k_{F2}, g_f, D_f, g_c and D_c are optimised. g_W, p_c and p_f are set to 1, n_W is set to 2 and V_W to 1.5. p_γ, g_γ and D_γ are set to 1, 1 and 50, respectively.

(ii) *ZmCLV3* expression domain. The optimisation aims at minimising the difference between *ZmCLV3* at equilibrium and C_t. A second component of the cost function ensures the expression domain of *ZmCLV3* increases with an increase of WUS.

The equilibrium of *ZmCLV3* is computed as follows:

$$w = diff(W)$$
$$l = diff(L1)$$
$$C = eq([l, w], [])$$
$$C_2 = eq([l, w \times 2], [])$$

and the cost function is:

$$E_C = mes(C, C_t, [C_t = 1, 2]) + 20\frac{C^6}{C_2^6}$$

The parameters k_l, k_w, g_w and D_w are optimised. V_C is set to 1.5, n_C to 10 and g_C to 1. p_w, p_l, g_l and D_l are set to 1.

(iii) ZmCLV3 peptide gradient. The first part of the optimisation used a hypothetical ZmCLV3 signal (c_h) produced by the manually defined *ZmCLV3* expression domain. As an equilibrium *ZmCLV3* domain has been computed, one can compute the corresponding equilibrium for the ZmCLV3 peptide. Optimising ZmCLV3 aims at minimising its difference with the previously computed c_h.

Equilibrium for ZmCLV3 follows:

$$c = diff(C)$$

and the cost function is:

$$E_c = mes(c, c_h)$$

Parameters g_c and D_c are re-optimised in this step.

(iv) *ZmCLV3/ZmWUS* feedback loop – Equilibrium of the complete model. As the previous steps of the optimisation independently found equilibria for components of the model, one has to ensure an adequate stable state exists also for the complete model. The feedback between *ZmWUS1* and *ZmCLV3* tends to induce dampened oscillations of the two genes. We propose an algorithm making use of that aspect and designed to quickly reach the equilibrium of the system using the parameter values obtained in the previous steps:

$E_d = \sum^i \left(\frac{dw_i}{dt}^2 + \frac{dc_i}{dt}^2\right)$

while $E_d > T_0$:

if $\sum^i \frac{dw_i}{dt}^2 < \sum^i \frac{dc_i}{dt}^2$:

$W = eq([A], [(c + f), (F_3 \times f)])$

$w = \frac{diff(W)+w}{2}$

$C = eq([l, w], [])$

$c = \frac{diff(C)+c}{2}$

else:

$C = eq([l, w], [])$

$c = \frac{diff(C)+c}{2}$

$W = eq([A], [(c + f), (F_3 \times f)])$

$w = \frac{diff(W)+w}{2}$

$E_d = \sum^i \left(\frac{dw_i}{dt}^2 + \frac{dc_i}{dt}^2\right)$

If E_d falls below a defined threshold T_0, the model is considered to have reached equilibrium. Additional numerical simulations confirm the equilibria are correctly found by this algorithm.

Behaviour of the model

Multiple optimisations resulted in 203 parameter sets successfully describing the wild type expression of *ZmWUS1* and *ZmCLV3*. In order to assess the ability of the model to describe perturbations of the system, a set of mutants were computed for all the optimised parameter sets:

- *Zmclv3*:

$$P_c \to 0$$

- *fea2*:

$$\frac{d[W]}{dt} \rightarrow V_W \times \frac{([\gamma][A])^{n_W}}{([\gamma][A])^{n_W} + k_A^{n_W}} \times \frac{k_{F_3}^{n_W}}{([F_3][f])^{n_W} + k_{F_3}^{n_W}} - g_W[W]$$

- *fea3:*

$$F_3 \rightarrow \mathrm{F}_3 \times 0$$

- *fea2/fea3:* implements both *fea2* and *fea3* mutations

- *fcp1:*

$$p_f \rightarrow 0$$

- *fcp1* over-expression:

$$p_f \rightarrow p_f \times 1.5$$

Both the wild type expression domains of *ZmWUS1* and *ZmCLV3* along with their expression in mutants are exemplified in **Supplementary Fig. 9**. The variation of the expression of the two genes, between wild type and mutant phenotypes and for all parameter sets, is presented in **Supplementary Fig. 10**.

fea2, *fea3* and *fea3; fea2* all lead to a substantial increase of both *ZmWUS1* and *ZmCLV3*, the model thus predicts a fasciated phenotype for the three mutants, which proves to be consistent with the experimental data presented in **Fig. 1**. Moreover, as shown, the severity of the phenotypes increases from *fea2* to *fea3* to *fea2/fea3*. Both the *fea3* and *fea3; fea2* mutants result in a large downward expansion of the *ZmWUS1* domain, similar to the *pZmWUS1-NLS.RFP* expression domain observed in *fea3* (**Fig. 2**).

fcp1 causes a large expansion of *ZmWUS1* and *ZmCLV3* and a predicted fasciated phenotype. The *ZmWUS1* domain exhibits a downward expansion typical of the *fea3* mutants.

Finally, over-expressing the *fcp1* peptide in its own expression domain (using a primordium specific YABBY promoter) causes a decrease of *ZmWUS1* expression, leading to a reduction of *ZmCLV3* expression. The phenotype suggests a smaller stem cell pool and thus a reduction of the meristem size or meristem arrest.

A notable aspect shared by all optimised parameter sets is the relatively weak feedback from *ZmCLV3* to *ZmWUS1* (*cf.* **Supplementary Fig. 10** – *zmclv3*, showing that *ZmWUS1* expression is mostly unaffected by the *zmclv3* phenotype). In order to achieve a correct *fea2* phenotype, the optimisation has to increase the expression of *ZmWUS1* when FEA2 receptors are lost. As the model allows both zmclv3 and fcp1 peptides to repress *ZmWUS1* expression, any balance of effects mediated by those two peptides could theoretically mediate the phenotype. However, after pooling all optimisation constraints together, resulting parameter sets mediate *fea2* phenotype mostly *via* fcp1. This is caused by the constraint on *fea3* phenotype, where *ZmWUS1* has to expand downward. Upon loss of FEA3 receptors, the expansion of *ZmWUS1* causes an expansion of the stem cell domain and an increase of the production of zmclv3. Would zmclv3 be a strong repressor of *ZmWUS1*, *ZmWUS1* would be repressed away from the tip of the meristem; this would contradict the experimental data presented on **Fig. 2d**. The solution to conciliate *fea2* and *fea3* phenotypes is to mediate *fea2* phenotype by fcp1 while tuning down the effect of zmclv3. This suggests that, in maize, the repression of *ZmWUS1* by the stem cell domain (mediated by zmclv3) may be weak or nonexistent, contrary to *A. thaliana*.

Together with the parameter values fixed in the optimization as described above, optimised parameter values used to exemplify the behaviour of the model in **Fig. 3** and **Supplementary Fig. 7-10** are:

$k_A = 0.0799349478204$

$k_{F_3} = 0.258483108091$

$k_{F_2} = 0.631322009895$

$g_f = 0.0989706220105$

$D_f = 0.315196037043$

$k_l = 0.35868731223$

$k_w = 1.28418451672$

$g_w = 10^{-5}$
$D_w = 3.05859740889$
$g_c = 1.41162777475$
$D_c = 0.795496002536$

"**Rice-like" model.**

The model described above is largely inspired by data obtained in *A. thaliana.* In particular, the *LOG* genes, whose expression patterns are unknown in maize, are expressed in the epidermis; in rice the expression resembles the stem cell domain[51]. In order to assess the importance of this choice we modified the model so the production of active cytokinin would not be limited to the epidermis, but to the tip of the meristem, as suggested from the data obtained in rice.

To assess this second model we followed the same procedure as described for the "Arabidopsis-like" model, both for the optimisation of the model and for the mutant analysis. The single difference between the two procedures is the source of cytokinin: L1 in the "Arabidopsis-like" model, *ZmCLV3* target in the "rice-like" model (**Supplementary Fig. 7**).

The "Rice-like" model correctly generates the *wild type* and mutant expression domains (**Supplementary Fig. 11**). This holds true for the 295 sets of parameters resulting from the optimisation procedure (**Supplementary Fig. 12**). Strikingly, the "rice-model" behaves extremely similarly to the "Arabidopsis model", suggesting that the pattern of expression of the *LOGs* in maize could be similar to either organisms without affecting the conclusions of the present study.

The model parameters exemplified in **Supplementary Fig. 11, 12** are:

$k_a = 0.0110285146717$
$k_{F_3} = 0.308187217119$
$k_{F_2} = 0.9037413184$
$g_f = 0.078395885527$

$$D_f = 0.256708058963$$

$$k_l = 0.358739560589$$

$$k_w = 0.723764685978$$

$$g_w = 1e-05$$

$$D_w = 5.3995729066$$

$$g_c = 0.697132853884$$

$$D_c = 0.519479366051$$

References

57. Winter, D. *et al.* An "Electronic Fluorescent Pictograph" browser for exploring and analyzing large-scale biological data sets. *PLoS One* **2**, e718 (2007).
58. Yadav, R.K., Girke, T., Pasala, S., Xie, M. & Reddy, G.V. Gene expression map of the Arabidopsis shoot apical meristem stem cell niche. *Proc Natl Acad Sci U S A* **106**, 4941-6 (2009).